SHIRSHOV INSTITUTE OF OCEANOLOGY

CRUISE REPORT No. 42

RV *AKADEMIK IOFFE* CRUISE 06 - 25 September 2013

North Atlantic Repeat Hydrography of sill sections between Greenland - Iceland - Faroe Islands and Shetlands

Principal Scientists **S Gladyshev**[1]

2014

Shirshov Institute of Oceanology
36 Nakhimovskii prospect
Moscow 117997 RUSSIA
Tel: +7(495) 719 0255 Fax: +7(499) 124 6342 Email:

sgladyshev@ocean.ru

[1]**Shirshov Institute of Oceanology**

DOCUMENT DATA SHEET

AUTHOR	***PUBLICATION DATE***
GLADYSHEV, S	2014
TITLE	
RV ***Akademik Ioffe*** Cruise 42 , 06 - 25 September 2013.	
REFERENCE	
Shirshov Institute of Oceanology, Akademik Ioffe Cruise Report, No. 42, 67pp. tables & figs.	

ABSTRACT

RV ***Akademik Ioffe*** Cruise 42 was a contribution to the RUSSIA CLIVAR Community Research Programme. The sections over North Atlantic sills between Greenland - Iceland - Faroe Islands and Shetlands were designed to estimate variability of the meridional fluxes and water mass exchange between the North Atlantic and the Arctic Ocean. The Denmark Strait section was repeated three times during six days to study short-term variability of the water mass properties circulation and meridional transport.

KEYWORDS

CRUISE 42 2013, *AKADEMIK IOFFE,* **CLIVAR, DENMARK STRAIT, NORTH ATLANTIC SILLS, INTEROCEAN EXCHANGE, CTD OBSERVATIONS, VMADCP, LADCP**

ISSUING ORGANISATION

Shirshov Institute of Oceanology
36 Nakhimovskii prospect
Moscow 117997 RUSSIA

Director: Academician Robert Nigmatulin

Copies of this report are available from: **Department of Marine Operations,** Tel: +7(495)7190255 Fax: +7(499)124 6342

Email: sgladyshev**@ocean.ru**

Contents

Scientific Personnel

GLADYSHEV, S.	Principal Scientist	Shirshov
TERESHCHENKOV, V.	Chief of CTD group	Shirshov
DOBROVOLSKII, M.	CTD, Sampling	Shirshov
ZAPOTYL'KO, V.	CTD, LADCP	Shirshov
SAVELIEV, V.	CTD, LADCP	Shirshov
PYATAKOV, V.	Sampling	Shirshov Atlantic Branch
KULESHOV, A.	Winch	Shirshov Atlantic Branch
LUKASHIN, S.	Winch	Shirshov Atlantic Branch
ALUYKAEVA, A.	Oxygen	Shirshov
KOLOKOLOVA, A.	Oxygen	Shirshov
BULYCHEV V.	Sampling	Shirshov Atlantic Branch
NECHVOLODOV, L.	Sampling	Shirshov
GLADYSHEVA, S.	Salinity	Shirshov

1. CRUISE NARRATIVE

1.1 Cruise Details

Expedition Designation: R/V ***Akademik Ioffe*** Cruise 42, RUSSIA CLIVAR

Principal Scientists: Dr Sergey V. Gladyshev (Shirshov).

Ship: RV ***Akademik Ioffe.***

Ports of Call: Kangerlussuaq (Greenland) to Rotterdam (Netherlands).

Cruise Dates: 06th September to 25th September 2013.

1.2 Cruise Summary

1.2.1 Cruise Track and Stations

The cruise track with station positions is shown in **Fig. l**. Only small volume samples were taken, details are listed in **Table 1**.

1.2.2. Equipment

The principal instruments used during the cruise were a SBE 9P-743 CTD with dual temperature and conductivity sensors (SBE 3 SN 03P5677, SBE 4 SN 042827, SBE 3 SN 03P4401, SBE 4 SN 042925), oxygen sensor (SBE 43, SN 430699, SN 430727), turbidity sensor (SeaPoint Turbidity, SN 10218 STM), Benthos altimeter model PSA-900D, LADCP WHS-300 kHz down-looking (S/N 6393), LADCP WHS-300 kHz up-looking (S/N 14151). These were mounted together with a multisampler Carousel SBE 32 equipped with 22 5-litre Niskin bottles. Upon recovery each bottle was sampled in turn for dissolved oxygen, nutrients, salinity. All sampling was done on deck. Currents were measured using vessel mounted ADCP (VMADCP) TRDI OS38 kHz (S/N 1185) installed at the central point of the ship hall.

Navigation information was provided by a Trimble SPSx50/SPSx51 - Modular GPS receiver and every second was recorded on the PC. Additional measurements were made with an ELAC 12 kHz, Aanderaa meteorological package.

1.2.3 Sampling

Nominal depths sampled were: bottom, 1100, 1000, 900, 800, 700, 600, 500, 400, 300, 200, 150, 100, 50, 30, 20, 10 m. On deep casts fewer shallow and intermediate bottles were fired. The actual bottle depths are shown in **Fig. 2**.

1.2.4 Number of Stations Occupied

103 stations (103 casts) were occupied during the cruise that includes sections between Greenland and Iceland (3 repeats), Faroe and Iceland, Shetlands and Faroe (3 repeats) (**Fig. l**).

1.3 Scientific Objectives

The cruise objectives were to:

1. To complete a CTD section from the Great Britain to Greenland.
2. To survey the North Atlantic sills with high-resolution CTD and LADCP/VMADCP data to determine the circulation and meridional fluxes.

1.4 Narrative

1.4.1 Introduction

The Meridional overturning circulation (MOC) in the North Atlantic is one of the main drivers of the widely known global oceanic "conveyor belt" – an important element of the Earth's climate system [e.g., van Aken, 2007]. Warm upper-ocean waters transported northward by the North Atlantic Current release heat to the atmosphere, gain density due to cooling and eventually sink in the subpolar North Atlantic and adjacent Arctic seas thereby generating the return southward flow of colder waters at depths (**Fig. 3**) [Dickson and Brown, 1994; Koltermann et al., 1999]. Temporal variability of the large-scale circulation and associated heat transport in the subpolar North Atlantic is one of the principal factors behind the high-latitude climate anomalies in the Northern Hemisphere.

Progress in understanding the causes of the ongoing climate change and forecasting climate variability in the Arctic and over European part of Russia for the next decades require reliable observation-based estimates of the variability of the North Atlantic circulation and the

Atlantic–Arctic heat and freshwater fluxes, as well as elucidation of the underlying mechanisms. In a number of recent studies, radical changes in the thermohaline regime and large-scale circulation in the Atlantic Ocean have been suggested to occur under global warming. For instance, the long-term freshening of the subpolar North Atlantic deep waters since the mid-1960s [Dickson et al., 2002] has been (cautiously) attributed to climate change-related factors [Curry et al., 2003; Hansen et al., 2004]. Hypothetically, under global warming, an increased evaporation in the tropics and increased precipitation at high latitudes, coupled with an intensified melting of Arctic ice, lead to the upper-ocean freshening in the regions of deep water formation and, hence, to the deep water freshening in the Atlantic Ocean. At the same time, milder winters along with the upper-ocean freshening lead to a decrease in the deep water production rates, which results in slowing of the Atlantic Meridional Overturning Circulation [e.g., Hansen et al., 2004; Bryden et al., 2005].

To better understand the past and present changes in the ocean-atmosphere dynamical system, as well as their causes and consequences, data on the full-depth oceanic variability are needed. An indispensable effective tool for assessing the large-scale circulation and thermohaline changes in the deep ocean and investigating mechanisms governing these changes are repeated full-depth transoceanic observations.

Since 1997, the P.P. Shirshov Institute of Oceanology has carried out the long-term monitoring of the North Atlantic circulation and water mass properties in the 59.5°N hydrographic section between Cape Farewell (Greenland) and Scotland (**Fig. 3**). Since 2002, the section has been repeated yearly on board the Russian research vessels, providing high precision data on temperature, salinity, oxygen and nutrients concentrations, and current velocities in the entire water column – "from shore to shore", from the sea surface to the bottom. In 2011, in addition to annual repeat measurements at 59.5°N, the P.P. Shirshov Institute of Oceanology started full-depth repeat observations of the oceanic exchange between the Atlantic and Arctic oceans through the straits between Greenland, Iceland, Faeroe and Shetland Islands (**Fig. 3**). The full-depth observations – of the same oceanic quantities as at 59.5°N – are performed in the straits from research vessels twice a year, in spring and fall. Based on the unique data set thus collected, a number of fundamental findings have already been achieved. Below, we briefly summarize the main subjects and results of our research.

The 59.5°N transatlantic section (**Fig. 3**) was designed for monitoring the large-scale circulation and thermohaline / chemical properties of oceanic waters at the northern periphery of the NA – the region where the warm upper-ocean waters are transformed by deep convection and mixing into the colder intermediate and deep waters – the Labrador Sea Water (LSW), Iceland Scotland Overflow Water (ISOW) and Denmark Strait Overflow Water (DSOW) (**Fig. 3**) – transported southward in the lower limb of the Atlantic MOC. Hydrographic data collected at 59.5°N along with those obtained within the framework of the kindred projects, primarily the French OVIDE (http://www.ifremer.fr/lpo/ovide), and historical data sets have been used for studying the dense water production [Falina et al., 2007; Falina et al., 2012], decadal temperature and salinity changes in the intermediate–deep water column [Sarafanov et al., 2007; Sarafanov et al., 2008; Sarafanov et al., 2010b], causes of these changes [Sarafanov, 2009; Sarafanov et al., 2010b], the mean state [Sarafanov et al, 2012] and long-term variability of the large-scale circulation in the region [Sarafanov et al., 2009; Sarafanov et al, 2010a; Våge et al., 2011].

1.4.2 Deep convection in the Irminger Sea

The oxygen data collected in 1997 in the northern North Atlantic in several sections ending nearby the southern tip of Greenland provided the observation-based support for the hypothesis [Pickart et al., 2003] that winter convection in the Irminger Sea may penetrate deep into the LSW layer (1000 – 2000 m) thus causing local renewal of this water mass. A separate lateral maximum of oxygen concentrations in the deep LSW layer was detected east of Cape Farewell (59.5°N, 36–40°W): the concentrations increased (by ~0.1 ml/l) from the Labrador Sea eastern edge toward the Irminger Sea (**Fig. 4**) rather than the reverse, as would be expected if LSW observed in the Irminger Sea interior in 1997 were solely of advective origin [Falina et al., 2007].

1.4.3. Reversal of the deep-water freshening

The LSW and Nordic Seas overflow-derived deep waters, ISOW and DSOW, freshened in the northern North Atlantic during the last three–four decades of the 20th century [Dickson et al., 2002]. Between the 1960s and 1990s, the water column in the region freshened on average by about 0.03 [Curry et al., 2003].

The long-term freshening reversed in the mid-1990s [Sarafanov et al., 2007; Sarafanov et al., 2008; Sarafanov et al., 2010b]. The salinification (and warming) of the intermediate and deep waters since the mid-1990s (**Fig. 5**) was much more intense than the preceding freshening. Over nearly a decade (1997–2006), temperature / salinity in the intermediate–deep water column ($\sigma_0 \geq 27.45$, depths > 500–1000 m) at 59.5°N increased by ~0.3°C / 0.03–0.04 [Sarafanov et al., 2008].

In the Irminger Sea, the long-term freshening in the deep water column (σ_0>27.80, depths > ~2000 m) reversed in the early 2000s [Sarafanov et al., 2010b]. The observed freshening reversal was a lagged consequence of the persistent ISOW salinification that occurred upstream, in the Iceland Basin, after 1996 due to salinification of the northeast Atlantic waters entrained into the overflow. It was demonstrated [Sarafanov et al., 2010b] that the entrainment salinity increase was associated with the North Atlantic Oscillation (NAO)-induced weakening and contraction of the Subpolar Gyre and corresponding northwestward advance of subtropical waters that followed the NAO decline in the mid-1990s and continued through the mid-2000s. Remarkably, the deep water freshening reversal was not related to changes in the overflow water salinity.

1.4.4. Deep-ocean salinity changes and the NAO

Close relationship between the thermohaline properties of the northern North Atlantic intermediate and deep waters and the winter NAO index on a decadal time scale ($r^2 \approx 0.65$, 1950s–2000s, **Fig. 6b** and **6c**) was revealed [Sarafanov, 2009] from the observation-based salinity time series for LSW in the Labrador Sea [Yashayaev, 2007] and ISOW in the Iceland basin [Boessenkool et al., 2007; Sarafanov et al., 2007]. Persistent NAO decline (amplification) leads to warming and salinification (cooling and freshening) in the intermediate–deep water column.

An explanation for the close link between the NAO and the coherent decadal changes in the intermediate and deep water properties in the region was proposed [Sarafanov, 2009]. The two factors dominate this link (**Fig. 6d**): (i) intensity of convection in the Labrador Sea controlling injection of relatively cold fresh waters into the intermediate layer and (ii) zonal extent of the Subpolar Gyre that regulates the relative contributions of cold fresh subpolar waters

and warm saline subtropical waters to the entrainment into the Norwegian Sea overflow south of the Iceland–Scotland Ridge and to the Atlantic inflow to the Nordic Seas. These factors act in phase leading to the observed coherent thermohaline changes in the intermediate–deep water column.

Due to weakening of the surface forcing associated with the NAO transition into neutral to low phase (1950s to mid-1960s, mid-1990s to mid-2000s), convection in the Labrador Sea weakens diminishing cold fresh water penetration into the intermediate layer. This results in warming and salinification at the intermediate depths in the Subpolar Gyre. Concurrently, the Subpolar Gyre contracts allowing northward advance of warm saline upper-ocean and intermediate subtropical waters in the northeastern North Atlantic. Northward progression of subtropical waters increases temperature and salinity at the upper intermediate levels and, correspondingly, increases temperature and salinity of the northeast Atlantic waters entrained into the Iceland–Scotland overflow along its pathway to the deep Iceland basin. As a result, temperature and salinity at the deep levels increase. The contrary changes – intensification of deep convection in the Labrador Sea and expansion of the Subpolar Gyre – caused by amplifying surface forcing (mid-1960s to mid-1990s) lead to cooling and freshening at the intermediate–deep levels. Additionally, under high-NAO conditions, deep convection may occur in the Irminger Sea potentially contributing to cooling and freshening at the intermediate (LSW) levels. The two regimes of convection and large-scale circulation corresponding to stronger (early 1990s) and weaker (mid-1960s, mid-2000s) NAO-related atmospheric forcing are schematically visualized in **Fig. 7**.

1.4.5 Deep-ocean salinity changes and climate change

There are increasing concerns that in the warmer climate, the MOC may substantially decline due to a decrease in the convective activity in the northern North Atlantic and Nordic Seas [e.g., Meehl et al., 2007]. The long-term freshening in the Nordic Seas and freshening of the northern North Atlantic deep waters in the 1960s–1990s have been considered as a likely indicator or precursor of the dramatic change in the MOC [e.g., Hansen et al., 2004]. The freshening has been attributed to a combination of factors potentially associated with the global warming: the increasing ice melt and net precipitation at high latitudes [e.g., Curry et al., 2003]. A probable causality between the climate change and the decreasing North Atlantic deep water

salinity has supported the concerns and unfavorable predictions, thus 'warming up' the reasonable scientific debate on climate change and overblown speculations in media.

Despite the long-term increase in freshwater input to the Arctic, freshening in the northern North Atlantic had reversed in the mid-1990s, as we demonstrated above. This reversal forces us to revise the hypotheses on the mechanisms behind the deep-water thermohaline anomalies. It seems doubtful that the persistent global temperature growth may lead to the opposite decadal trends (positive-then-negative-then-positive, **Fig. 6**) in the deep water salinity.

Our results [Sarafanov et al., 2008; Sarafanov, 2009; Sarafanov et al., 2010b] suggest that natural atmospheric variability over the North Atlantic plays the major role in the deep-water thermohaline variability on a decadal time scale. There are no reasons to associate the deep-water freshening in the 1960s–1990s with climate change, unless the 3-decade-long surface forcing amplification is evidently shown to be a consequence of the latter. Having said that, the net 1950s–2000s trends in the water mass salinities are negative implying that the global factors (e.g., probable intensification of hydrological cycle [Curry et al., 2003]) may act on longer time scales.

1.4.6 Decadal variability of the Deep Western Boundary Current at Cape Farewell

Recent decadal changes in the Deep Western Boundary Current (DWBC) transport southeast of Cape Farewell were assessed from hydrographic data (1991–2007, **Fig. 7a**), direct velocity measurements (2002–2006) and satellite altimetry (1992–2007). Following the approach used in earlier studies [e.g., Bacon, 1998], we first determined that the DWBC (σ_0>27.80) baroclinic transport (T_{BC}) referenced to 1000 m depth increased by ~2 Sv between the mid-1990s (1994–1997) and 2000s (2000–2007) (**Fig. 8b**) [Sarafanov et al., 2009]. In the next step, we quantified velocity changes at the reference level (1000 m) by combining estimates of the hydrography-derived velocity changes in the water column and the altimetry-derived velocity changes at the sea surface [see Sarafanov et al., 2010a]. The inferred increase in the southward velocity at 1000 m above the DWBC in 1994–2007 indicates that the increase in the DWBC absolute transport was larger but very close to the 2-Sv increase in the DWBC T_{BC}. This result along with the observed coherence of the DWBC absolute and baroclinic transport changes between individual observations [Sarafanov et al., 2010a] imply that the DWBC absolute

transport variability in the region is well represented by its baroclinic component on decadal and shorter time scales.

The historical record of the DWBC T_{BC} (1955–2007, **Fig. 8c**) updated after Bacon [1998] shows distinct decadal variability (±2–2.5 Sv) with the transport minima in the 1950s and mid-1990s, maximum in the early 1980s and moderate-to-high transport in the 2000s. The DWBC T_{BC} decadal variability is consistent with the general pattern of the recent decadal hydrographic and circulation changes in the northern North Atlantic. The DWBC T_{BC} anomalies negatively correlate (R = –0.80, 1955–2007) with thickness anomalies of the Labrador Sea Water (LSW) at its origin implying a close link between the DWBC transport southeast of Cape Farewell and the LSW production in the Labrador Sea (**Fig. 8d**). During the recent three decades (late 1970s – late 2000s), the DWBC T_{BC} changes were also in-phase with changes in the strength and zonal extent of the Subpolar Gyre [see Sarafanov et al., 2010a]. In particular, the Gyre weakening at shallow levels in the mid-1990s – mid-2000s was accompanied by the DWBC strengthening in the Irminger Sea [Sarafanov et al., 2009; Sarafanov et al., 2010a; Våge et al., 2011]. The results imply that the decadal changes in the (i) LSW production, (ii) SPG strength and (iii) DWBC transport in the Irminger Sea are linked, representing a complex coherent oceanic response to the decadal variability of the surface forcing.

1.4.7 Mean state of the full-depth circulation in the 2000s

A mean state of the full-depth summer circulation in the Atlantic Ocean in the region in between Cape Farewell (Greenland), Scotland and the Greenland-Scotland Ridge (see **Fig. 3**) was assessed by combining 2002–2008 yearly hydrographic measurements at 59.5°N, mean dynamic topography, satellite altimetry data and available estimates of the Atlantic–Nordic Seas exchange [see Sarafanov et al., 2012]. The mean absolute transports by the upper-ocean, mid-depth and deep currents and the MOC (MOCσ=16.5±2.2 Sv, at σ_0=27.55) at 59.5°N were quantified in the density space. Inter-basin and diapycnal volume fluxes in between the 59.5°N section and the Greenland-Scotland Ridge were then estimated from a box model.

The estimated meridional and diapycnal volume fluxes contributing to the MOC are schematically visualized in **Fig. 9**. The dominant components of the meridional exchange across 59.5°N are the North Atlantic Current (NAC, 15.5±0.8 Sv, σ_0<27.55) east of the Reykjanes Ridge, the northward Irminger Current (IC, 12.0±3.0 Sv) and southward Western Boundary

Current (WBC, 32.1±5.9 Sv) in the Irminger Sea and the deep water export from the northern Iceland Basin (3.7±0.8 Sv, σ_0>27.80). About 60% (12.7±1.4 Sv) of waters carried in the MOCσ upper limb (σ_0<27.55) by the NAC/IC across 59.5°N (21.1±1.0 Sv) recirculates westwards south of the Greenland-Scotland Ridge and feeds the WBC. 80% (10.2±1.7 Sv) of the recirculating NAC/IC-derived upper-ocean waters gains density of σ_0>27.55 and contributes to the MOCσ lower limb. Accordingly, the contribution of light-to-dense water conversion south of the Greenland-Scotland Ridge (~10 Sv) to the MOCσ lower limb at 59.5°N is one and a half times larger than the contribution of dense water production in the Nordic Seas (~6 Sv).

1.4.8 Cascading of dense shelf waters in the Irminger Sea

Based on the hydrographic data collected at 59.5°N, 64.3°N and 65–66°N in the western Irminger Sea in the 1990s – 2000s, an observational evidence for the deep-reaching cascading of dense shelf waters south of the Denmark Strait was found [Falina et al., 2012]. The data collected in the northwestern Irminger Sea (65–66°N) indicate that the East Greenland Current ~200 km south of the Denmark Strait occasionally carries shelf waters as dense as the overflow-derived deep waters transported by the DWBC (σ_0 > 27.80). Hydrographic traces of cascading of dense shelf waters down the East Greenland slope were found from repeat measurements at 64.3ºN, where the densest fresh plumes were observed within the DWBC (σ_0 > 27.80) (**Fig. 10**). Using the data collected at 59.5°N, we showed that the fresh 'signals' originating from the shelf can be traced in the DWBC as far downstream as the latitude of Cape Farewell, where the anomalously fresh oxygenated plumes are repeatedly observed in the ISOW and DSOW density classes.

The results of our analysis along with the results from earlier studies [e.g., Rudels et al., 1999; Rudels et al., 2002] indicate that shelf water cascading in the northern Irminger Sea is an intermittent process occurring in all seasons of the year. This implies that, despite the apparent short duration of a particular cascading event, the cumulative contribution of such events to the thermohaline variability and southward export of the deep waters in the WBC can be considerable. Our tentative estimate based on data from two synoptic surveys at ~59.5°N suggests that the transient contribution of a cascading event in the northern Irminger Sea to the DWBC transport at Cape Farewell can be as large as ~25%.

References

1. Bacon, S. (1998), Decadal variability in the outflow from the Nordic seas to the deep Atlantic Ocean, *Nature*, *394*, 871–874.
2. Dickson, R. R., and J. Brown (1994), The production of North Atlantic Deep Water: Sources, rates and pathways, *J. Geophys. Res.*, *99*, C6, 12319–12341.
3. Dickson, R., Yashayaev, I., Meincke, J., Turrell, B., Dye, S., and J. Holfort (2002), Rapid freshening of the deep North Atlantic Ocean over the past four decades, *Nature*, *416*, 832–837.
4. Boessenkool, K. P., Hall, I. R., Elderfield, H., and I. Yashayaev (2007), North Atlantic climate and deep-ocean flow speed changes during the last 230 years, *Geophys. Res. Lett.*, *34*, L13614, doi:10.1029/2007GL030285.
5. Curry, R., Dickson, R., and I. Yashayaev (2003), A change in the freshwater balance of the Atlantic Ocean over the past four decades, *Nature*, *426*, 826–829.
6. Falina, A., A. Sarafanov, and A. Sokov (2007), Variability and renewal of Labrador Sea Water in the Irminger Basin in 1991–2004, *J. Geophys. Res.*, *112*, C01006, doi: 10.1029/2005JC003348.
7. Falina A., A. Sarafanov, H. Mercier, P. Lherminier, A. Sokov, and N. Daniault (2012), On the cascading of dense shelf waters in the Irminger Sea, *J. Phys. Oceanogr.*, doi:http://dx.doi.org/10.1175/JPO-D-12-012.1 (in press)
8. Hansen, B., Osterhus S., Quadfasel D., and W. Turrell (2004), Already the day after tomorrow?, *Science*, *305*, 953–954.
9. Hurrell, J. W. (1995), Decadal trends in the North Atlantic Oscillation: regional temperatures and precipitation, *Science*, *269*, 676–679.
10. Koltermann, K. P., A. Sokov, V. Tereschenkov, S. Dobroliubov, K. Lorbacher, and A. Sy (1999), Decadal changes in the thermohaline circulation of the North Atlantic, *Deep Sea Res.*, *Part II*, *46*, 109–138, doi:10.1016/S0967-0645(98)00115-5.
11. Lherminier, P., H. Mercier, T. Huck, C. Gourcuff, F. F. Perez, P. Morin, A. Sarafanov, and A. Falina (2010), The Atlantic Meridional Overturning Circulation and the subpolar gyre observed at the A25–Ovide section in June 2002 and 2004, *Deep-Sea Res.*, *Part I*, *57*, 1374–1391, doi:10.1016/ j.dsr.2010.07.009.

12. Meehl, G. A., (2007), Global climate projections. Climate Change 2007: The Physical Science Basis, S. Solomon et al., Eds., Cambridge University Press, 747–847.
13. Pickart, R. S., Spall, M., Ribergaard, M. H., Moore, G. W. K. and R. Milliff (2003), Deep convection in the Irminger Sea forced by the Greenland tip jet, *Nature*, *424*, 152–156.
14. Rudels B., Eriksson P., Grönvall H., Hietala R. and Launiainen J. (1999), Hydrographic Observations in Denmark Strait in Fall 1997, and their Implications for the Entrainment into the Overflow Plume, *Geophys. Res. Lett.*, *26*, 1325–1328.
15. Rudels, B., E. Fahrbach, J. Meincke, G. Budeus, and P. Eriksson (2002), The East Greeenland Current and its contribution to the Denmark Strait overflow, *ICES J. Marine Science*, *59*, 1133–1154.
16. Sarafanov, A., A. Sokov, A. Demidov, and A. Falina (2007), Warming and salinification of intermediate and deep waters in the Irminger Sea and Iceland Basin in 1997–2006, *Geophys. Res. Lett.*, *34*, L23609, doi:10.1029/2007GL031074.
17. Sarafanov, A., A. Falina, A. Sokov, and A. Demidov (2008), Intense warming and salinification of intermediate waters of southern origin in the eastern subpolar North Atlantic in the 1990s to mid-2000s, *J. Geophys. Res.*, *113*, C12022, doi:10.1029/2008JC004975.
18. Sarafanov, A. (2009), On the effect of the North Atlantic Oscillation on temperature and salinity of the subpolar North Atlantic intermediate and deep waters, *ICES J. Marine Science*, *66 (7),* 1448–1454, doi:10.1093/icesjms/fsp094.
19. Sarafanov, A., A. Falina, H. Mercier, P. Lherminier, and A. Sokov (2009), Recent changes in the Greenland–Scotland overflow-derived water transport inferred from hydrographic observations in the southern Irminger Sea, *Geophys. Res. Lett.*, *36*, L13606, doi:10.1029/2009GL038385.
20. Sarafanov A., A. Falina, P. Lherminier, H. Mercier, A. Sokov, and C. Gourcuff (2010a), Assessing decadal changes in the Deep Western Boundary Current absolute transport southeast of Cape Farewell (Greenland) from hydrography and altimetry, *J. Geophys. Res.*, *115*, C11003, doi:10.1029/2009JC005811.
21. Sarafanov A., H. Mercier, A. Falina, A. Sokov, and P. Lherminier (2010b), Cessation and partial reversal of deep water freshening in the northern North Atlantic: observation-

based estimates and attribution, *Tellus*, *62A*, 80–90, doi:10.1111/j.1600-0870.2009.00418.x.

22. Sarafanov A., A. Falina, H. Mercier, A. Sokov, P. Lherminier, C. Gourcuff, S. Gladyshev, F. Gaillard, and N. Daniault (2012), Mean full-depth summer circulation and transports at the northern periphery of the Atlantic Ocean in the 2000s, *J. Geophys. Res., 117,* C01014, doi:10.1029/2011JC007572.
23. Schmitz, W. J., Jr., and M. S. McCartney (1993), On the North Atlantic Circulation, *Rev. Geophys.*, *31*, 29–49.
24. Schott, F. A., and P. Brandt (2007), Circulation and deep water export of the subpolar North Atlantic during the 1990s, *in Ocean Circulation: Mechanisms and Impacts*, *Geophys. Monograph Series*, *173*, Eds. A. Schmittner, J. Chiang, and S. Hemmings, 91–118, doi:10.1029/173GM08.
25. Sutherland, D. A., and R. S. Pickart (2008), The East Greenland Coastal Current: structure, variability, and forcing, *Prog. Oceanogr.*, *78*, 58–77, doi:10.1016/j.pocean.2007.09.006.
26. Våge K., R. Pickart, A. Sarafanov, Ø. Knutsen, H. Mercier, P. Lherminier, H. van Aken, J. Meincke, D. Quadfasel, and S. Bacon (2011a), The Irminger Gyre: circulation, convection, and interannual variability, *Deep-Sea Res. Part I*, *58*, 590–614, doi:10.1016/j.dsr.2011.03.001.
27. van Aken, H. M. (2007), The oceanic thermohaline circulation: An introduction, New York, Springer, 326 p., ISBN 978-0-387-36637-1.
28. Yashayaev, I. (2007), Hydrographic changes in the Labrador Sea, 1960–2005, *Prog. Oceanogr.*, *73*, 242–276.

.

1.5 Preliminary Results

The upper-ocean, mid-depth and deep water circulation patterns, merging the results of the present analysis with those from the earlier studies [e.g., *Macrander et al.*, 2005; *Østerhus et al.*, 2005, 2008; *Schott and Brandt*, 2007; *Sutherland and Pickart*, 2008; *Lherminier et al.*, 2010; *Våge et al.*, 2011], are schematically visualized Figures 12–14. A schematic diagram of the meridional overturning circulation in the Atlantic Ocean north of 59.5°N is displayed in Fig. 9.

The results provide the following conceptual view of the gyre / overturning circulation at the northern periphery of the Atlantic Ocean in the 2000s.

The NAC and IC collectively carry 21.1 ± 1.0 Sv of warm upper-ocean waters across 59.5°N northwards within the MOCσ upper limb ($\sigma_0 < 27.55$). About 40% of this flow forms the Atlantic Inflow to the Nordic Seas, and 60% (12.7 ± 1.4 Sv) recirculates westwards in the subpolar gyre northern limb south of Iceland to feed the WBC in the Irminger Sea. Only 20% (2.4 ± 1.2 Sv) of the recirculating NAC/IC-derived waters exits the Irminger Sea in the WBC at shallow levels ($\sigma_0 < 27.55$), while 80% (10.2 ± 1.7 Sv, a half of the NAC/IC northward flow across 59.5°N) gains density of $\sigma_0 > 27.55$ and enters the MOCσ lower limb. The resulting net southward transport in the MOCσ lower limb at the latitude of Cape Farewell is 16.5 ± 2.2 Sv, of which ~60% (~10.2 Sv) is due to light-to-dense water transformation south of the GSR.

As no dense-to-light water re-conversion is expected to occur in the subpolar gyre, the NAC/IC-derived waters, once entering the MOCσ lower limb in the Irminger Sea, will eventually contribute to the MOCz lower limb (~11 Sv at 59.5°N) at the southern margin of the subpolar region. There, at ~48°N, the MOCσ and MOCz are of nearly the same magnitude, 16 ± 2 Sv, as estimated from data collected in the 1990s [see *Schott and Brandt*, 2007; *Lumpkin et al.*, 2008]. This is very close to our estimate of the mean MOCσ at 59.5°N. The comparison is tentative, though, because it does take into account the decadal variability of the MOC [*Koltermann et al.*, 1999; *Willis*, 2010]. With this caveat in mind, our results imply a minor contribution to the MOCσ by the net dense water formation in the subpolar gyre between ~48°N and 59.5°N. This inference concurs with the results by *Pickart and Spall* [2007] suggesting a

minor contribution to the Atlantic MOC by the net water mass transformation in the Labrador Sea.

To conclude, the results of the present study, verified with independent estimates where possible, provide the first observation-based quantitative view of a mean state of the gyre / overturning circulation at the northern periphery of the Atlantic Ocean. The most interesting features of the obtain circulation pattern are as follows:

• Nearly half of volume of the upper-ocean waters transported northward across 59.5°N in the eastern limb of the subpolar gyre (NAC and IC, $\sigma_0 < 27.55$) overturns in the density plane south of the GSR and feeds the lower limb of the Atlantic MOCσ.

• The contribution to the MOCσ lower limb at 59.5°N by overturning (light-to-dense transformation) of the NAC / IC-derived upper-ocean waters south of the GSR is one and a half times as large as the contribution of the Nordic Seas overflows.

• The net southward flow in MOCσ lower limb at 59.5°N is associated primarily with the deep water ($\sigma_0 > 27.80$) export. Nearly half of the net southward flow of deep waters across 59.5°N is due to entrainment of the Atlantic waters in the Irminger Sea.

• The DWBC at 59.5°N is fed primarily by the Denmark Strait Overflow and by the diapycnal flux / entrainment from the mid-depth layer, while the contribution to the DWBC transport from the ISOW flow is minor. A major part of the ISOW transported into the Irminger Sea from the Charlie-Gibbs Fracture Zone recirculates southward in the eastern Irminger Sea and exits the basin via an interior pathway rather than along the western boundary. The results can be used for validation of numerical models. From this perspective, multi-year mean transports have an obvious advantage over individual section-based synoptic estimates, which bear the impress of vigorous variability occurring on a variety of spatial and temporal scales. The methodological outcome is that the combined use of repeat hydrography, the MDT by *Rio and Hernandez* [2004] and satellite altimetry data can provide a useful estimate of the mean full-depth circulation across a transatlantic section without imposing *a priori* constraints.

1.6 Major Problems and Goals Not Achieved

The CTD pump S/N 053895 was replaced with S/N 053903 after sta. 3130 due to its bad performance (noisy data of the primary sensors). SBE 9plus #743 was replaced with spare SBE 9plus #767 after station #3132. Bottle #4 did not close on sta. ##3065, 3097, 3100 and 3132 because of cock release mechanism problem. Bottle # 10 periodically leaked. We had to stop cast for a few minutes during sta. 3101, 3121, 3123 and 3136 because of the ship maneuvering due to large cable angle. Station #3052 was repeated because of the large cable angle up to 20°. SEASAVE closed on sta. 3082 during up cast at depth 70 m.

2. CONTINUOUS MEASUREMENTS (on station and underway)

2.1 Navigation

Navigation data from Trimble SPSx50/SPSx51 GPS was recorded every 1 second and was stored on the PC in binary format.

2.2 Meteorological Measurements

The standard mean meteorological measurements were stored in the separate files on the same PC with navigation data. Recording were running immediately after departure from Kangerlussuaq (Greenland) on 06th September, and worked reliably until completion of the cruise in Rotterdam (Netherlands) on 25th September.

2.3 Thermosalinograph

SBE 21 S/N 3254 data were collected along the section line starting on September 12th.

2.4 Echosounding

The bathymetric equipment aboard during RV Akademik Ioffe Cruise 42 consists of an ELAC 12 kHz hydrographic echosounder. Data were collected for most of the cruise. The Hull mounted transducer is located 5.8 metres below the sea surface and this value was entered to estimate the depth.

Depth was indicated on the echosounder display and stored on the PC together with the navigation.

Two files with extension NAV and MET with maximum size 256032 b were created. File name corresponded to GMT time when the file was opened for records.

2.5 Vessel Mounted Acoustic Doppler Current Profiler (VMADCP) OS 38 kHz

The Ocean Surveyor 38 kHz is designed for vessel-mount current profile measurement in the upper ocean water from depths greater than 40-50 meters. The system consists of a transducer and electronics chassis connected to PC. Data are transmitted in binary format through the I/O cable. GPS data in NMEA format are transmitted separately to another PC COM – port. The VMADCP can operate in two regimes (Narrow Bandwith and Broad Bandwith Profiling). Its main specifications are shown below.

To collect OS 38 kHz data we used *VmDas* software (version 1.46). The NMEA messages *VmDas* reads are standard GGA, HDG, HDT, VTG messages.

	Bin size	Maximum range	Accuracy $(cm/s)^2$
NarrowBand (long-range mode)	16 m	800 - 1000 m	30
	24 m	900 - 1200 m	23
BroadBand (high-precision mode)	16 m	520 - 730 m	12
	24 m	730 – 780 m	9

We used a following configuration to collect the data.

NP00001 – Narrow Bandwidth profiling

NN060 – number of bins 60

NS1600 – cell size 24 m

NF1600 – blanking size 16 m

BP00 – no bottom track (BP),

VmDas saves data in a few files with extension ENX, ENS, ENR (raw data with and without navigation), NR – NMEA messages, STA and LTA averaged data. Misalignment angle was introduced in configuration file and was used by VmDas for data correction.

Data processing performed STA files with 40-profile averaging. Taking into account that single ping takes about 3 seconds, one 40-profile ensemble lasts near 120 seconds in Narrow Bandwidth regime.

Data processing consists of data conversion in NetCDF format with extension NC and further cleaning, filtering, tide removing (using barotropic tidal model TPXO 7.2) and averaging. The standard space averaging was 3 km. IFREMER software was used to process OS 38 kHz data.

3. ON-STATION MEASUREMENTS

3.1 CTD

3.1.1 Equipment

The deep profiler system used during the cruise included the following components: SBE 32 painted aluminum 24 bottle multisampler frame, SBE 9P-0743 CTD, spare SBE 9P-0767, CTD Up and Down looking RD Instruments WHS – 300 kHz Acoustic Doppler Current Profiler (LADCP), Separate Battery pack pressure case ext. 6000 m connected to LADCPs with star cable, 24 x 5 litre Test Oceanic Niskin bottles, Benthos altimeter PSA-900D.

Lab equipment for data acquisition and archiving of CTD/LADCP data consisted of the following items mounted on the deck.

Pentium IV – Intel 2.2 GHz, PC Intel Core 2 Duo 2.4GHz Personal Computers. APC Back-UPS 550VA/330W, SBE 11p Deck Unit.

Cruise Preparation

Equipment and sensors were assembled when the ship turned around Greenland (07-11th September). Water bottles were checked for integrity of seals, taps, stoppers and lanyards before being fitted and roped to the multisampler frame.

Deployment

The CTD performed well during the cruise with little evident instrument drift and good accuracy.

The CTD was deployed with a lowering rate of 60 metres/min (30-40 metres/min in the upper 200 metres or deeper if the conditions are rough). It is recovered at a rate of 60 metres/min.

The LADCPs fitted within the frame with a separate battery pressure case performed well. These units contain a compass and tilt sensors which could possibly provide useful information on the attitude and rotation of the whole profiler package throughout deployments.

Bottle firing using the deck unit and pylon was very reliable during the cruise.

Operationally this has been a successful cruise with virtually no time being lost due to mechanical or equipment failure.

3.1.2 Data processing and calibration

CTD data were logged at 24 scans per second and passed from the CTD deck unit to the PC.

The CTD data was recorded onto disk by the PC using SEABIRD SEASOFT-Win 32: Seasave 7, Software Release 7.21d. A screen display of temperature, oxygen, salinity and density profiles vs pressure are used to decide the depths at which bottles are to be tripped on the up cast. The bottles are tripped using the enable and fire buttons on the PC screen. During post-processing, the SEASAVE software stores 35 scans at each bottle trip within a separate file. At the end of the station, all the data and header files associated with the station are transferred immediately via ethernet to the second PC. The SBE data processing software is used to create 1 dbar processed data files.

The data processing takes the following steps:

DATCNV Converts the raw data to physical parameters.

WILDEDIT For every block of 100 scans, flags all scans whose pressure, temperature, conductivity and oxygen values differ from the mean by more than 2 standard deviations. Recomputes mean from unflagged data then marks as bad all scans exceeding 20 standard deviations from these new values.

FILTER Low pass filter pressure channel with time constant used for pressure 0.150 seconds.

ALIGNCTD Aligns the oxygen values relative to the pressure values accounting for the time delays in the system. Time offsets of 4.000 secs for oxygen are used.

CELLTM A recursive filter used to remove the thermal mass effects from the conductivity data. Thermal anomaly amplitude and time constants of 0.0300 and 7.0000 were used.

LOOPEDIT Marks as bad, all cycles on the down trace for which the vertical velocity of the CTD unit is less than 0.25 metres/sec.

WINDOW FILTER cosine filter temperature and conductivity, window size 23 scans.

DERIVE Computes salinity, potential temperature, sigma-t, sigma theta and oxygen values.

BINAVG Averages the down cast into 1 dbar pressure bins.

SPLIT Splits the data into DOWN and UP cast.

Calibration data

The CTD calibrations used during this cruise were supplied by Sea Bird Electronics and are as follows:

Pre-cruise calibration:

CALIBRATION DATE: 01-Aug 2013 (sta. 3040-3132)

Conductivity Sensor S/N 042827

g = -1.0038388 1 e +001
h = 1.3710686 9 e +000
i = 1.4481873 5 e -004
j = 5.1968474 5 e -005
CPcor = -9.5700e-008
CTcor = 3.2500e-006

Post-cruise calibration:
CALIBRATION DATE: 24-Jun 2014 (sta. 3040-3132)
Conductivity Sensor S/N 042827
g = -1.00348848e+001
h = 1.36977079e+000
i = 5.01531580e-004
j = 2.74090064e-005
CPcor = -9.570 0 e -008 (nominal)
CTcor = 3.250 0 e -006 (nominal)
Average drift between *pre* and *post-cruise* calibrations: -0.00010 PSU/month (at 3.0 S/m)

CALIBRATION DATE: 04-Jan 2012 (sta. 3133-3141)
Conductivity Sensor S/N 042968 (SBE 9plus #767)
g = -1.0256497 2 e +001
h = 1.3888025 5 e +000
i = 1.7664232 1 e -004
j = 6.2895383 5 e -005
CPcor = -9.5700e-008
CTcor = 3.2500e-006

Post-cruise calibration:
CALIBRATION DATE: 24-Jun 2014 (sta. 3133-3141)
Conductivity Sensor S/N 042968 (SBE 9plus #767)
g = -1.02539270e+001
h = 1.38755405e+000
i = 5.79001510e-004
j = 3.28989341e-005
CPcor = -9.570 0 e -008 (nominal)
CTcor = 3.250 0 e -006 (nominal)
Average drift between *pre* and *post-cruise* calibrations: -0.00010 PSU/month (at 3.0 S/m)

Pre-cruise calibration:
CALIBRATION DATE: 27-Sep-12 (sta. 3040-3132)
Temperature Sensor S/N 035677
Temperature ITS-90 = 1/{g + h[*ln*(f0/f)] + i[*ln*2(f0/f)] + j[*ln*3(f0/f)]} - 273.15 (°C)
Following the recommendation of JPOTS: T68 is assumed to be 1.00024 * T90 (-2 to 35°C)
f is the frequency
g =4.29391849e-003
h =6.23531754e-004
i =1.89302750e-005
j =1.40036300e-006
f0 = 1000.0

Post-cruise calibration:
CALIBRATION DATE: 19-Jun-14 (sta. 3040-3132)
Temperature Sensor S/N 035677
Temperature ITS-90 = 1/{g + h[*ln*(f0/f)] + i[*ln*2(f0/f)] + j[*ln*3(f0/f)]} - 273.15 (°C)
Following the recommendation of JPOTS: T68 is assumed to be 1.00024 * T90 (-2 to 35°C)
f is the frequency
g = 4.29395484e-003
h = 6.23609246e-004
i = 1.89843091e-005
j = 1.41258435e-006
f0 = 1000.0
Average drift between *pre* and *post-cruise* calibrations: +0.00000 degrees Celsius/year

Pressure Sensor S/N 89105 (sta. 3040-3132) no drift
CALIBRATION DATE: 27-June-11
C1 = -4.9053 7 1 e+004
C2 = -1.2105 9 4 e+000
C3 = 1.4283 5 0 e-002
D1 = 3.9016 0 0 e-002
D2 = 0.0000 0 0 e+000
T1 = 3.0010 1 7 e+001
T2 = -5.7583 8 4 e-004
T3 = 4.2101 2 0 e-006
T4 = 2.2654 0 0 e-009
T5 = 0.0000 0 0 e+000)
AD590M = 1.28912e-002
AD590B = -8.43097e+000
Slope = 0.99995
Offset = 1.4284 (dbars)

Oxygen Sensor 430699 (sta. 3040 -3132)
CALIBRATION DATE: 08-Dec-2014 (sta. 3040-3132)
$Oxygen(ml/l) = \{Soc * (V + Voffset)\} * Oxsat (T,S) * e^{(Tcorr*T)} * e^{(Pcor*P)}$

Where:
V = SBE 43 output voltage signal (volts)
T = CTD temperature (°C)
S = CTD salinity (psu)
P = CTD pressure (dbars)
Oxsat(T,S) = oxygen saturation (ml/l)
Soc, Voffset, tcor, and *pcor* are calibration coefficients

Let:
$\varphi = Oxsat (T,S) * e^{(Tcorr*T)} * e^{(Pcor*P)}$
$Oxygen(ml/l) = Soc * (V + Voffset) * \varphi$
$Oxygen(ml/l)/ \varphi = Soc * (V + Voffset) = M * V + B$
Where:
Soc = M
Voffset = B / M

In our case for sill sections

Soc = 4.2843e-001
Tau = 0.0
Boc = 0.0000
Voffset = -0.4370
tcor = 0.001700
pcor = 1.35e-004

3.1.3 Final Post-Cruise CTD Calibrations

Temperature Calibration Temperature Sensors S/N 035677 (SBE 9P-0743), S/N 034423 (SBE 9P-0767)

We applied zero correction for the primary sensors **S/N 035677** and **S/N 034423** and we used *pre-cruise calibration coefficients* for all stations of the cruise).

Pressure Calibration Pressure Sensor S/N 89105

Final CTD pressure correction: Since no drift for pressure sensor was defined by SeaBird Electronics pressure was corrected for atmospheric pressure only. With offset in *.con* or *.xmlcon* file set to -0.0026 db, pressure measured by CTD should equal barometric pressure

• Calculate offset (db) = barometer reading – CTD reading

– Conversion of psia to decibars: decibars = (psia - 14.7) * 0.6894759

• Enter calculated offset in *.con* or *.xmlcon* file

• Example:

– CTD reads -2.5 dbars

– Barometer reads 14.65 psia.

Converting to decibars, barometer reads (14.65 - 14.7) * 0.6894759 = -0.034 dbars

– offset (db) = barometer reading – CTD reading = -0.034 - (-2.5) = 2.466

Salinity Calibration Conductivity Sensor S/N 042827

We used *pre-cruise calibration coefficients* for sta. 3040-3132 of the cruise corrected by -+0.0003 PSU (sensor slope correction 1.0000077). This drift was also defined by taking 246 salinity samples from depth deeper than 300 m between 12 and 22 September 2013. These samples were measured with Autosal 8400 B laboratory salinometer (S/N 67465) during 5 runs between 13 and 23 September. The results of these measurements are shown in **Fig. 11a**.

Although we defined slightly larger sensor drift of order 0.001 PSU during the cruise it was however within the accuracy of our measurements in the ship laboratory.

Salinity Calibration Conductivity Sensor S/N 042968

We used *pre-cruise calibration coefficients* for all stations of the cruise corrected by -+0.0036 PSU (sensor slope correction 1.0000910). This drift was defined by taking 20 salinity samples from depth deeper than 300 m on 22nd September 2013. These samples were measured with Autosal 8400 B laboratory salinometer (S/N 67465) during last run on 23rd September. The results of these measurements are shown in **Fig. 11b**.

Description of Equipment and Technique

Salinity samples are analyzed on Guildline Autosal model 8400 B salinometer. Samples are drawn in 150 ml dark glass medicine bottles. All bottles were equipped with plastic liners and caps. The salinometer cell is filled and rinsed three times with sample water before readings are recorded. Minimum three salinometer readings were recorded for every sample and standardization. If the values are fluctuating, more readings are taken.

Sampling Procedure and Data Processing Technique

Salinity samples are drawn into 150 ml medicine bottles after three rinses. The bottles are filled up to the shoulders and then capped with caps with plastic liners. Files for each separate run are prepared. These files consist of various metadata (date, cruise, lab temperature, geographic location, operator, etc.) and sample specific data such as the bath temperature, sample ID number, and average conductivity ratio. A PC based program computes the salinity using average conductivity ratio of the runs and the standard IAPSO formula. Any changes in the salinometer readings between successive standardizations are assumed to have occurred as a linear drift of the instrument. Thus, the program applies a correction to the ratios, which varies linearly with the samples analyzed. The salinity data is then placed in the water sample database.

Laboratory and Sample Temperatures

Full cases of samples are taken from the winch room to the salinometer lab where they are left for a period of at least 24 hours to equilibrate to laboratory temperature before being analyzed.
The bath in the salinometer was kept at 21°C.

Standards Used

The salinometer was standardized using IAPSO standard water, Batch P152, dated May, 2013. Standardization with a new bottle was carried out at the beginning and end of the run as well as after 50 bottle samples.

3.1.4 SBE 43 Dissolved Oxygen Sensor Calibration using Winkler Titrations

We use a method for statistically estimating calibration coefficients for calculating dissolved oxygen in milliliters per liter from SBE 43 output voltage. The technique requires dissolved oxygen concentration in ml/l (determined from Winkler titration of water samples) and SBE 43 oxygen voltage outputs at the times the water samples were collected. Sea-Bird's data processing software, SBE Data Processing, is used to produce a data table suitable for the analysis.

Background

The equation used in Sea-Bird's software for calculating dissolved oxygen in ml/l from SBE 43 output voltage is a form of that given in Owens-Millard (1985):

$$Oxygen(\ ml/l) = \{Soc * (V + Voffset + tau * \partial V/\partial t) + Boc * e^{(-0.03*T)}\} * Oxsat\ (T,S) * e^{(Tcorr*T)} * e^{(Pcor*P)} \qquad eqn\ 1$$

Where:
V = SBE 43 output voltage signal (volts)
$\partial V/\partial t$ = time derivative of SBE 43 output signal (volts/second)
T = CTD temperature (°C)
S = CTD salinity (psu)
P = CTD pressure (dbars)
$Oxsat(T,S)$ = oxygen saturation (ml/l)
Soc, Boc, Voffset, tau, tcor, and *pcor* are calibration coefficients

Characterization of the SBE 43 in the laboratory and ocean suggest that the most accurate results are obtained by setting *Boc* and *tau* to zero. Equation 1 then reduces to:

$$Oxygen(\ ml/l) = \{Soc * (V + Voffset)\} * Oxsat\ (T,S) * e^{(Tcorr*T)} * e^{(Pcor*P)} \qquad eqn\ 2$$

The SBE 43 is expected to provide an output voltage that is linear with respect to oxygen concentration. Normal calibration drift manifests itself as a loss of sensitivity and is evident as a change of slope and offset in the linear relationship between oxygen concentration and voltage output. The coefficients *tcor* and *pcor* correct for small secondary responses to temperature and pressure. Because these coefficients change very slowly over time, the values given on the SBE 43 calibration certificate are used in this analysis.

Setting *Boc* and *tau* to zero, we will rearrange equation 2 into a linear form and perform a linear regression to obtain a new *Soc* and *Voffset*.

Let:

$$\varphi = Oxsat\ (T,S) * e^{(Tcorr*T)} * e^{(Pcor*P)}$$

The oxygen equation then reduces to:

$$Oxygen(\ ml/l) = Soc * (V + Voffset) * \varphi$$

This may be expressed in a linear form as shown in equation 3 below. A linear regression is calculated using Winkler oxygen concentration divided by φ as the dependent variable and SBE 43 output voltage as the independent variable.

$$Oxygen(\ ml/l)/\varphi = Soc * (V + Voffset) = M * V + B \qquad eqn\ 3$$

Where:
Soc = M
Voffset = B / M

Winkler oxygen divided by φ versus SBE 43 output voltage for this cruise is shown in **Fig. 12** and includes a linear regression line calculated from the data.

The *Soc* value is 4.2843e-001.
The *Voffset* value is -0.4370 for the sill sections

964 oxygen samples were used to build this linear fits.

We cannot build the single fit for SBE 43 0727 (sta. 3133-3141) because of low statistics and adjusted each oxygen CTD profile separately.

Procedure

As a first step, extract pressure, temperature, salinity, oxygen saturation, and SBE 43 voltage from the parts of your CTD data collected when the water sampler closures occurred.

We run SBE Data Processing, and select Data Conversion in the Run menu. Select the appropriate configuration (*.con*) and data (*.dat*) files on the *File Setup* tab. In the *Data Setup* tab we set *Convert data from* to *Upcast and downcast* and *Create file types* to *Create bottle (.ros) file only*.

To extract CTD data concurrent to the water sampler closures, Data Conversion must know when the closures occurred. Select an appropriate *Source of scan range data*, depending on your instrument type and how the sampler was commanded to close bottles:

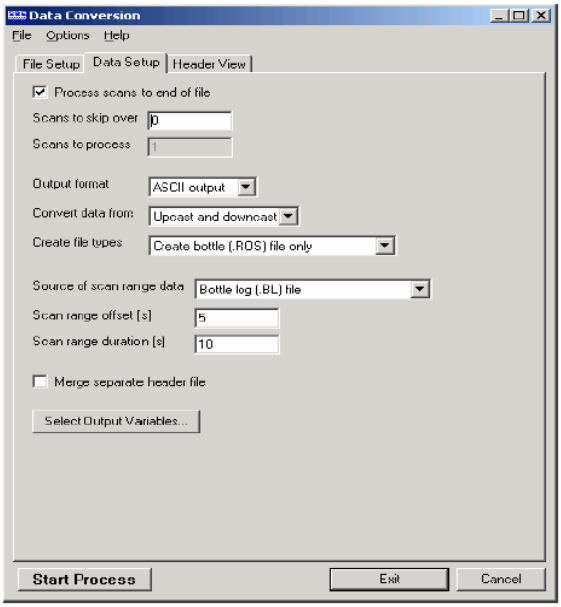

• SBE 9*plus* with SBE 11*plus* - The data stream is marked with a *bottle confirm* bit each time a closure occurred.
• Using SEASAVE to operate the water sampler - A *.bl* file, with scan ranges corresponding to closures, is created during the cast.

Like all sensors, the SBE 43 has a finite response time to a change in dissolved oxygen concentration. This response time is usually on the order of 6 seconds. For this reason, good sampling procedure dictates that the instrument package should be stopped in the water column long enough for the SBE 43 and all other sensors to completely equilibrate before closing the water sampler. An equilibration time of 5 to 6 response times, or 30 to 36 seconds, is adequate. We used to wait 30 seconds.

Data Conversion is extracting data 5 seconds before each water sampler closure and will extract 10 seconds of data. Note that 10 seconds is longer than the SBE 43 response time. Because we are extracting data for 5 seconds after the water sampler closure, the instrument package must remain stopped for at least this long.

To estimate *Soc* and *Voffset*, we need pressure, temperature, salinity, oxygen saturation (ml/l), and SBE 43 Oxygen Voltage to go with each Winkler titration data value. We use *Select Output Variables* and add each of the required parameters; the dialog box is shown below.

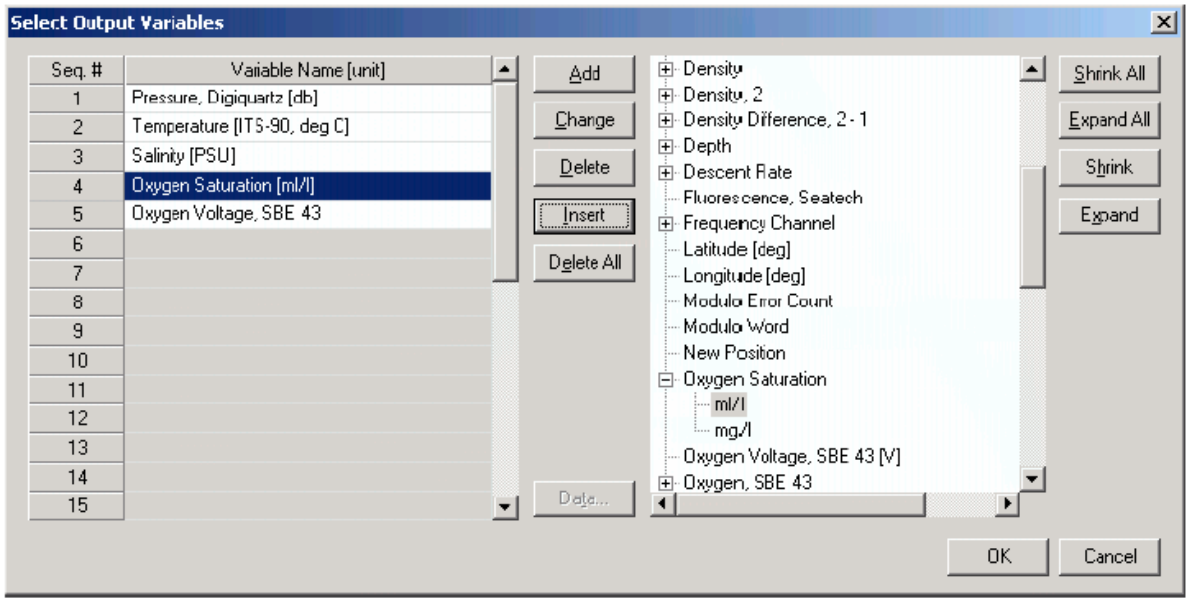

After selecting all the variables, click *OK* to return to the Data Conversion Data Setup tab. Then click *Start Process* to create the *.ros* file.

In our case, the *.ros* file contains 10 seconds of data centered on the moment the bottle closure occurred for every bottle closure. To make a useful table, we select Rosette Summary from SBE Data Processing's Run menu. Rosette Summary calculates averages and standard deviations for the variables selected in Data Conversion. Select the appropriate *.con* and *.ros* files on the *File Setup* tab. To average the data in the *Data Setup* tab we click the *Select Averaged Variables* button; after selecting all the variables, click *OK* to return to the Rosette Summary Data Setup tab. Then click *Start Process* to create a data table file with the *.btl* extension.

Further, we run a program READBTLDATA to create a file with average pressure, temperature, salinity, oxygen saturation, and SBE 43 output voltage for each water sampler closure depth, by importing the *.btl* file and the Winkler titration dissolved oxygen values from our titration log, matching water sampler closures to number of station, bottle number and

pressures. The program also calculates φ, using *tcor* and *pcor* from the SBE 43 calibration sheet.

Then, calculate *Winkler* O_2 / φ.

Using the table we perform a linear regression, with:
• *Winkler* O_2 / φ (shown as Winkler/phi in the table) as the *Y* data
• SBE 43 output voltages as the *X* data

Reference

Owens, W. B., and R. C. Millard Jr., 1985: A new algorithm for CTD oxygen calibration. J. Physical Oceanography, 15, 621-631.
(NOTE: calibration expressed as ml/l)

3.2 Oxygen Bottle Samples

Oxygen samples were drawn first from every bottle. Duplicate samples were taken on each cast, usually from the first two bottles. Samples were drawn into clear, wide necked calibrated glass bottles and fixed on deck with reagents dispensed using Aquastep bottle top dispensers. A test station used to check on the oxygen bottle calibrations and as an opportunity to train a number of people to take the samples. The samples were shaken on deck and again in the laboratory 1/2 hour after collection, when the bottles were checked for the tightness of the stoppers and presence of bubbles. The samples were then stored under water until analysis.

Bottle temperatures were taken, following sampling for oxygen, using a hand held electronic thermometer probe. The temperatures were used to calculate any temperature-dependent changes in the sample bottle volumes.

Samples were analyzed in the constant temperature laboratory, starting three hours after sample collection, following the Winkler whole bottle titration with an amperometric method of endpoint detection, as described by Culberson (1991). The equipment used was supplied by Metrohm and included the Titrino unit and control pad, exchange unit with 10 ml burette to dispense the thiosulphate in increments of 2 μl , with an electrode for amperometric end point detection.
The difference for the duplicate pairs sampled on each station was in a range 0.00-0.03 ml/l (Table 2).

The thiosulphate normality was checked on each run and recalculated every time the reservoir was topped up against potassium iodate. The exact weight of this standard, the calibrated 5 ml exchange unit driven by a Metrohm Dosimat and the 1L glass volumetric flask used to dispense and prepare the standard.

The introduction of oxygen with the reagents and impurities in the manganese chloride were corrected for by blank measurements made on each run, as described in the WOCE Manual of Operations and Methods (Culberson, 1991).

Collected data shows that dissolved oxygen concentrations varied from 5.36 to 8.72 ml/l. In order to control the accuracy of the oxygen measurements at almost each cast were taken parallel sample from one bottle.

Reproducibility of measurements

1273 samples were taken during the cruise; in addition, 77 duplicates were analyzed. Statistics on the duplicates are given in Table 2. These include both duplicates taken from the same bottle (replicates) and those taken from different bottles fired at the same depth. The data gave a standard deviation of 0.005 ml/l, or 0.07%.

References:

Culberson, C.H. 1991.15 pp in the WOCE Operations Manual (WHP Operations and Methods) WHPO 91/1, Woods Hole.

Modern methods of hydrochemical research of the ocean, 1992. IO RAS, Moscow (in Russian).

(A. Kolokolova)

3.3 Lowered Acoustic Doppler Current Profiler (LADCP)

The TRDI WHS 300 kHz ADCPs consists of a pressure case rated to 6000 metres with 4 transducers at one end in a convex arrangement and the beams diverging at 20 degrees from the vertical. At the opposite end to the transducers is a connector that enables downloading of data and connects it to other pressure cases containing another ADCP and the power supply pack. This arrangement allowed the ADCPs and the battery pack to be mounted vertically as up and down-looking on the CTD frame. Connection amongst all units was established using star cable with three male and two female terminations. Two male cable ends were always attached to the frame, this enabled comms leads to be readily connected pre and post deployment.

Communications: The 20-m communication leads (which also allow external power to be supplied to the ADCP) were sufficiently long to route it through to the port side of the deck lab where it was connected to a dedicated PC and external power supply. The latter was set at 48+ volts and was left on whilst the ADCP was on deck. 5 minutes prior to deployment the external power supply was shut off, the

instrument checked and the configuration file sent to the ADCP as described in the manual instructions. The free end of the fly leads was greased and the end cap refitted, this was then taped to the frame for security.

Post deployment: When the CTD/LADCP was brought inboard, the fly-lead connectors were dried and the comms leads were connected to them. This stopped undue bending of the cables and kept them clear of the water bottles, aiding sampling. External power was applied again and the cast data downloaded as per the manual with a baud rate of 57600. The processing is accomplished using software developed by Visbeck after transferring the data to the PC.

Battery power was supplied to the ADCP in the form of 42 volts from 28 x 1.5 volt alkaline cells. Four of these packs were available for the cruise, as the ADCP will function at a minimum of 32 volts this was deemed an adequate stock for the duration.

Data quality: The data quality from the ADCP was good throughout. Due to the bad weather instrument titles sometimes exceeded 12° and this data was rejected during processing.

The LADCPs seem to function well and generates useful information on currents. The battery supply has its limitations though and thought should be given to alternatives to the present set-up.

3.3.1 LADCP Processing for Current Profiles

A brief account of the LADCP current data processing, file nomenclature and directory structure is provided in the following lines. Little emphasis is put into a detailed description of the main programming tools used, since these are part of a standard software package developed by Gerd Krahmann (version 10.13).

Outline of LADCP current calculation method

The Broad Band LADCP used during AI42 cruise was designed to measure the instantaneous relative velocities of scatterers in the water column by taking advantage of the Doppler frequency shift, phase changes and correlation between coded pulses transmitted and received by the LADCP's four transducers. Conversion of this raw data stream to a profile of absolute currents involved an elaborate calculation method.

Firstly, Doppler shifts needed to be scaled to velocity units by taking into account the depth-dependent sound velocity (estimated from CTD T and S measurements). Directions could be inferred from trigonometric calculations based on the geometry of the transducer set, the orientation of the package (measured with a flux gate compass) and the local magnetic declination. The depth of the instrument was calculated from the integration of the measured vertical velocity and later adjusted to match the depth given by the CTD's pressure sensor.

The velocities corresponding to each single ensemble (or, in effect, to each transducer ping) were gridded in bins of depth set 10 meters. Statistical rejection of spiky measurements within each of these bins followed.

In order to reject the unwanted motion of the instrument (but also the barotropic component of the current), shear profiles were calculated for each ensemble. A complicated editing scheme preceded this shear calculation. A final shear profile (baroclinic current) was derived by real- depth gridding of the shear profiles calculated for individual ensembles. It was hoped that any relative velocities introduced by the high-frequency motion of the CTD package would be smoothed out by this repeated averaging.

The barotropic component of the flow was finally calculated from bottom-tracking measurements (bottom-track mode) or, in most occasions, in an integral sense from differential GPS positions of the ship (water-track mode).

The definitive velocity profile was hence obtained as the sum of the baroclinic and barotropic components.

During AI42 cruise, no specific error calculation was performed. Profiles of shear standard deviation were included in the cast log sheet folder. Internal wave signals were obvious throughout the cruise.

Relevant PC files

The raw data were downloaded from the LADCP into a devoted PC after each cast and stored as a binary file called vNNNNm_01.000 for Master and vNNNNs_01.000 for Slave the c:\ladcp\AI42\dNNN directory, where NNNN stands for the CTD cast number, e.g. raw data from cast 3131 were stored in the files d:\AI42\data\ladcp\v3131m_01.000 and v3131s_01..000.

The configuration files (named Mconf.txt and Sconf.txt) containing the operating instructions (setting of track mode, bin depth, etc.) given to the LADCP previously to deployment was stored in the same directory.

Text files of the form NNNNm.log and NNNNs.log are the log of the 'bbtalk' session (testing the state and functioning of the instrument) previous to deployment. The details of the sessions for every single cast in the cruise are to be found in the cast log sheets.

A whole variety of files were created and manipulated during the different processing stages, and no mention will be made of the majority of them for reasons of clarity. The processing procedure may be summarised in two steps:

1- create CTD pressure, temperature and salinity data file as well as navigation collected every second in order to obtain the best possible estimates of depth and sound velocity. This is done using 'SBE Data Processing software and ConvLADCP Fortran program.

2- use the Gerd Krahmann's standard matlab package (v. 10.13) with P. Lherminier's improvements (IFREMER) to process LADCP and CTD data

References

M. Visbeck 1994: Deep Velocity Profiling using Lowered Acoustic Doppler Current Profiler: Bottom Track and Inverse Solutions J. Atmos. Oceanic Technol. 10, 764-773.

4. CRUISE LOGISTICS

Mobilization

Mobilization for the cruise took place on the way from Kangerlussuaq (Greenland) to the first station of the cruise. It took six days. The scientific team arrived at the ship on September 06th.

ACKNOWLEDGEMENTS

The principal scientists would like to thank the Master, officers, crew and scientists of the RV Akademik Ioffe for making this such an enjoyable, as well as successful cruise.

TABLES

FIGURES

Fig. l. Station location and ship track (in red). The shelf area with depth less than 200 m is shaded.

Fig.2. Vertical distribution of samples along the sill sections.

Fig. 3. Schematic diagram of the large-scale circulation in the northern North Atlantic compiled from [Schmitz and McCartney, 1993; Schott and Brandt, 2007; Sutherland and Pickart, 2008; Lherminier et al., 2010]. Abbreviations for the main topographic features, currents and water masses are explained in the legend. The nominal locations of the 59.5°N hydrographic section (1997 – present) and sections across the straits between Greenland, Iceland, Faeroe and Shetland Islands (2011 – present) are shown with the solid green lines.

Fig. 4. Oxygen concentrations (ml/l) in the water column (lower panel) as observed in March–October 1997 in four hydrographic sections (upper panel) ending nearby the southern tip of Greenland. A separate oxygen maximum in the LSW layer (1000–2000 m) in the Irminger Sea at 59.5°N strongly implies local convective renewal of LSW before 1997. Adapted from [Falina et al., 2007].

Fig. 5. Warming and salinification in the northern North Atlantic between the mid-1990s and mid-2000s, as observed at 59.5°N. The figure shows the 2006–1997 temperature (°C, left) and salinity (right) differences on isobaric surfaces in the Irminger Sea and Iceland Basin. Adapted from [Sarafanov et al., 2007].

Fig. 6. Coherence of the decadal salinity changes (1950s – 2000s) of the intermediate (LSW) and deep (ISOW) waters in the northern North Atlantic and their link to the North Atlantic Oscillation (NAO) index. **(a)** Schematic representation of the LSW and ISOW pathways and locations of the Icelandic Low (L) and Azores High (H) centers constituting the NAO dipole pattern. The red dotted line indicates the 59.5°N transatlantic section. **(b)** Salinity time series for LSW in the Labrador Sea [Yashayaev, 2007] and ISOW in the Iceland basin [Boessenkool et al., 2007; Sarafanov et al., 2007] overlaid by the third order polynomial fits. **(c)** Time series of the winter NAO index, after [Hurrell, 1995], overlaid by 7-year running mean and third order polynomial fit. **(d)** Mechanism of the NAO effect on the decadal changes in temperature (T) and salinity (S) of the northern North Atlantic intermediate and deep waters. Positive / negative links shown with the dark / light grey arrows mean that changes in ‘causative’ and ‘consequential’ characteristics have the same / opposite sign(s). The overall effect of the NAO on T and S of the in the water column is negative: persistent NAO decline leads to warming and salinification of the water masses and vice versa, as shown in (b) and (c). Adapted from [Sarafanov, 2009].

Fig. 7. Schematic representation of the upper-ocean circulation and convection intensity in the northern North Atlantic under high (left) and low (right) NAO conditions. Blue (magenta) solid arrows indicate the upper-ocean flows with higher fraction of colder fresher subpolar (warmer saltier subtropical) waters. The main pathways of the Nordic overflow-derived deep waters are shown with the dotted curves. "C" and "E" symbols are used to denote, respectively, the deep convection sites and the domain, where the Atlantic waters are entrained into ISOW. Larger (smaller) circles indicate stronger (weaker) convection. SPG and STG – the subpolar and subtropical gyres, respectively. Adapted from [Sarafanov, 2009].

Fig. 8. The Deep Western Boundary Current (DWBC) transport variability and its link to the convection intensity in the Labrador Sea. **(a)** Locations of the hydrographic sections (1991–2007) and schematic of the deep water circulation in the Irminger Sea. **(b)** The DWBC transport anomalies at Cape Farewell in 1991–2007, 1 Sv = 10^6 m^3 s^{-1}. The 1994–1997 and 2000–2007 mean anomalies and the 1994–2007 linear trends are shown. **(c)** Anomalies of the DWBC transport at Cape Farewell and the Labrador Sea Water (LSW) thickness in the Labrador Sea in the 1950s–2000s. **(d)** Correlation coefficient (R^2) for the two times series shown in **(c)** at the 0–5-year lag, the LSW thickness leads. The correlation maximum is achieved at the 1–3-year lag. The DWBC transport anomalies in the southern Irminger Sea are foregone by the convection intensity anomalies in the Labrador Sea. Adapted from [Sarafanov et al., 2009].

Fig. 9. Schematic diagram of the Meridional Overturning Circulation (MOC) at the northern periphery of the Atlantic Ocean, northeast of Cape Farewell. The dotted lines refer to the σ_0 isopycnals 27.55 and 27.80. The arrows denote the integral meridional and diapycnal volume fluxes. Where the signs are specified, the positive (negative) transports are northward (southward). The NAC and EGIC transports in the upper layer ($\sigma_0 < 27.55$) at 59.5°N are the throughputs accounting for the recirculations. EGIC – the East Greenland / Irminger Current – refers to the upper part of the Western Boundary Current. Other abbreviations are explained in the legend to **Fig. 3**. Adapted from [Sarafanov et al., 2012].

Fig. 10. Salinity observed in the northwestern Irminger Sea at 64.3°N in February 1998. The σ_0 isopycnals 27.55, 27.70, 27.80 and 27.88 are plotted as the thick black lines; the station locations are marked with the ticks on the top axis. The plot shows fresh dense waters descending (cascading) down the continental slope of Greenland down to the LSW layer ($27.70 < \sigma_0 < 27.80$) and the layer of the Nordic Seas overflow-derived deep waters ($\sigma_0 > 27.80$). Adapted from [Falina et al., 2012].

Fig. 11. Autosal 8400B CTD salinity difference for primary (in black) and secondary (in red) conductivity sensors based on 860 salinity samples measurements (16 runs) during 38 cruise of R/V *Akademik Ioffe*. Vertical bars show standard deviation of each run.

Fig. 12. Regression line for Winkler oxygen divided by φ versus SBE 43 output voltage the sill sections, (b) 59.5 section.

Fig. 13. The vertical distribution of (a) potential temperature and (b) salinity and (c) dissolved oxygen between Greenland and Iceland 12-14 September 2013. Density is shown in black.

Fig. 14. The vertical distribution of (a) potential temperature and (b) salinity and (c) dissolved oxygen between Iceland and Faroe Islands 20-21 September 2013. Density is shown in black.

Fig. 15. The vertical distribution of (a) potential temperature and (b) salinity between Shetlands and Faroe Islands 21-23 September 2013. Density is shown in black.

.

Table 1

R/V Ak. Ioffe CRUISE 42

STATION	CAST	TYPE	DATE	TIME	CODE	LATITUDE	LONGITUDE	NAV	DEPTH	BOTTOM	BOTTLES	COMMENTS
3040	1	ROS	091213	1107	BE	67 23.8 N	033 02.7 W	GPS	286	3	12	CTD,LADCP,O2
3040	1	ROS	091213	1127	BO	67 23.4 N	033 02.6 W	GPS	286	3	12	CTD,LADCP,O2
3040	1	ROS	091213	1152	EN	67 22.9 N	033 01.9 W	GPS	286	3	12	CTD,LADCP,O2
3041	1	ROS	091213	1248	BE	67 19.9 N	032 43.9 W	GPS	421	2	14	CTD,LADCP,O2
3041	1	ROS	091213	1304	BO	67 19.7 N	032 44.1 W	GPS	421	2	14	CTD,LADCP,O2
3041	1	ROS	091213	1330	EN	67 19.6 N	032 43.8 W	GPS	421	2	14	CTD,LADCP,O2
3042	1	ROS	091213	1433	BE	67 15.5 N	032 23.6 W	GPS	368	3	13	CTD,LADCP,O2
3042	1	ROS	091213	1453	BO	67 15.0 N	032 22.1 W	GPS	368	3	13	CTD,LADCP,O2
3042	1	ROS	091213	1519	EN	67 15.1 N	032 21.8 W	GPS	368	3	13	CTD,LADCP,O2
3043	1	ROS	091213	1632	BE	67 10.1 N	032 00.4 W	GPS	300	5	11	CTD,LADCP,O2
3043	1	ROS	091213	1652	BO	67 10.0 N	031 58.7 W	GPS	300	5	11	CTD,LADCP,O2
3043	1	ROS	091213	1712	EN	67 10.1 N	031 58.5 W	GPS	300	5	11	CTD,LADCP,O2
3044	1	ROS	091213	1822	BE	67 05.2 N	031 37.6 W	GPS	291	3	12	CTD,LADCP,O2
3044	1	ROS	091213	1842	BO	67 04.9 N	031 35.6 W	GPS	291	3	12	CTD,LADCP,O2
3044	1	ROS	091213	1859	EN	67 04.8 N	031 35.3 W	GPS	291	3	12	CTD,LADCP,O2
3045	1	ROS	091213	2018	BE	67 00.1 N	031 13.4 W	GPS	358	5	15	CTD,LADCP,O2
3045	1	ROS	091213	2034	BO	66 59.9 N	031 12.7 W	GPS	358	5	15	CTD,LADCP,O2
3045	1	ROS	091213	2053	EN	66 59.7 N	031 12.5 W	GPS	358	5	15	CTD,LADCP,O2
3046	1	ROS	091213	2215	BE	66 55.1 N	030 50.2 W	GPS	583	3	16	CTD,LADCP,O2
3046	1	ROS	091213	2233	BO	66 55.1 N	030 49.9 W	GPS	583	3	16	CTD,LADCP,O2
3046	1	ROS	091213	2259	EN	66 55.1 N	030 50.2 W	GPS	583	3	16	CTD,LADCP,O2
3047	1	ROS	091313	0032	BE	66 50.0 N	030 27.4 W	GPS	417	7	14	CTD,LADCP,O2
3047	1	ROS	091313	0049	BO	66 50.1 N	030 27.0 W	GPS	417	7	14	CTD,LADCP,O2
3047	1	ROS	091313	0108	EN	66 50.3 N	030 27.1 W	GPS	417	7	14	CTD,LADCP,O2
3048	1	ROS	091313	0243	BE	66 45.1 N	030 03.6 W	GPS	329	5	13	CTD,LADCP,O2
3048	1	ROS	091313	0259	BO	66 45.1 N	030 03.3 W	GPS	329	5	13	CTD,LADCP,O2
3048	1	ROS	091313	0317	EN	66 45.2 N	030 03.6 W	GPS	329	5	13	CTD,LADCP,O2
3049	1	ROS	091313	0449	BE	66 39.8 N	029 39.2 W	GPS	296	2	12	CTD,LADCP,O2
3049	1	ROS	091313	0504	BO	66 39.8 N	029 39.0 W	GPS	296	2	12	CTD,LADCP,O2
3049	1	ROS	091313	0521	EN	66 39.8 N	029 39.2 W	GPS	296	2	12	CTD,LADCP,O2
3050	1	ROS	091313	0648	BE	66 35.0 N	029 16.7 W	GPS	307	5	12	CTD,LADCP,O2
3050	1	ROS	091313	0703	BO	66 34.9 N	029 16.3 W	GPS	307	5	12	CTD,LADCP,O2

3050	1	ROS	091313	0725	EN	66 34.8 N	029 16.0 W	GPS	307	5	12	CTD,LADCP,O2
3051	1	ROS	091313	0851	BE	66 29.9 N	028 54.5 W	GPS	326	9	14	CTD,LADCP,O2
3051	1	ROS	091313	0905	BO	66 29.9 N	028 54.5 W	GPS	326	9	14	CTD,LADCP,O2
3051	1	ROS	091313	0928	EN	66 30.0 N	028 55.1 W	GPS	326	9	14	CTD,LADCP,O2
3052	1	ROS	091313	1100	BE	66 25.1 N	028 31.9 W	GPS	301	1	1	CTD,LADCP,O2
3052	1	ROS	091313	1119	BO	66 25.2 N	028 31.9 W	GPS	301	1	1	CTD,LADCP,O2
3052	1	ROS	091313	1126	EN	66 25.2 N	028 32.2 W	GPS	301	1	1	CTD,LADCP,O2
3052a	1	ROS	091313	1129	BE	66 25.3 N	028 32.3 W	GPS	310	4	13	CTD,LADCP,O2
3052a	1	ROS	091313	1137	BO	66 25.3 N	028 32.7 W	GPS	310	4	13	CTD,LADCP,O2
3052a	1	ROS	091313	1158	EN	66 25.3 N	028 33.2 W	GPS	310	4	13	CTD,LADCP,O2
3053	1	ROS	091313	1336	BE	66 20.0 N	028 08.8 W	GPS	341	4	13	CTD,LADCP,O2
3053	1	ROS	091313	1352	BO	66 20.0 N	028 08.2 W	GPS	341	4	13	CTD,LADCP,O2
3053	1	ROS	091313	1414	EN	66 20.2 N	028 08.2 W	GPS	341	4	13	CTD,LADCP,O2
3054	1	ROS	091313	1530	BE	66 14.9 N	027 45.8 W	GPS	470	5	16	CTD,LADCP,O2
3054	1	ROS	091313	1548	BO	66 14.8 N	027 45.3 W	GPS	470	5	16	CTD,LADCP,O2
3054	1	ROS	091313	1620	EN	66 14.6 N	027 44.9 W	GPS	470	5	16	CTD,LADCP,O2
3055	1	ROS	091313	1756	BE	66 09.2 N	027 15.4 W	GPS	512	6	15	CTD,LADCP,O2
3055	1	ROS	091313	1817	BO	66 09.1 N	027 15.2 W	GPS	512	6	15	CTD,LADCP,O2
3055	1	ROS	091313	1846	EN	66 09.1 N	027 15.9 W	GPS	512	6	15	CTD,LADCP,O2
3056	1	ROS	091313	1938	BE	66 05.3 N	027 03.0 W	GPS	652	4	18	CTD,LADCP,O2
3056	1	ROS	091313	2004	BO	66 05.0 N	027 03.0 W	GPS	652	4	18	CTD,LADCP,O2
3056	1	ROS	091313	2030	EN	66 04.9 N	027 03.0 W	GPS	652	4	18	CTD,LADCP,O2
3057	1	ROS	091313	2130	BE	66 01.2 N	026 47.9 W	GPS	452	5	12	CTD,LADCP,O2
3057	1	ROS	091313	2148	BO	66 01.0 N	026 48.2 W	GPS	452	5	12	CTD,LADCP,O2
3057	1	ROS	091313	2204	EN	66 01.0 N	026 48.3 W	GPS	452	5	12	CTD,LADCP,O2
3058	1	ROS	091313	2325	BE	65 56.2 N	026 29.3 W	GPS	284	4	8	CTD,LADCP,O2
3058	1	ROS	091313	2341	BO	65 55.8 N	026 29.2 W	GPS	284	4	8	CTD,LADCP,O2
3058	1	ROS	091313	2354	EN	65 55.7 N	026 29.3 W	GPS	284	4	8	CTD,LADCP,O2
3059	1	ROS	091413	0136	BE	65 50.1 N	026 00.2 W	GPS	222	5	7	CTD,LADCP,O2
3059	1	ROS	091413	0148	BO	65 49.9 N	025 59.8 W	GPS	222	5	7	CTD,LADCP,O2
3059	1	ROS	091413	0157	EN	65 49.9 N	025 59.6 W	GPS	222	5	7	CTD,LADCP,O2
3060	1	ROS	091413	0318	BE	65 45.0 N	025 38.7 W	GPS	268	4	8	CTD,LADCP,O2
3060	1	ROS	091413	0329	BO	65 44.9 N	025 38.3 W	GPS	268	4	8	CTD,LADCP,O2

3060	1	ROS	091413	0342	EN	65 45.0 N	025 37.9 W	GPS	268	4	8	CTD,LADCP,O2
3061	1	ROS	091413	0502	BE	65 40.1 N	025 16.3 W	GPS	89	4	4	CTD,LADCP,O2
3061	1	ROS	091413	0514	BO	65 40.0 N	025 15.6 W	GPS	89	4	4	CTD,LADCP,O2
3061	1	ROS	091413	0519	EN	65 40.0 N	025 15.4 W	GPS	89	4	4	CTD,LADCP,O2
3062	1	ROS	091413	0635	BE	65 35.1 N	024 55.1 W	GPS	66	6	3	CTD,LADCP,O2
3062	1	ROS	091413	0646	BO	65 34.9 N	024 54.9 W	GPS	66	6	3	CTD,LADCP,O2
3062	1	ROS	091413	0651	EN	65 34.9 N	024 55.0 W	GPS	66	6	3	CTD,LADCP,O2
3063	1	ROS	091413	0820	BE	65 40.0 N	025 15.9 W	GPS	85	12	5	CTD,LADCP,O2
3063	1	ROS	091413	0827	BO	65 39.8 N	025 15.7 W	GPS	85	12	5	CTD,LADCP,O2
3063	1	ROS	091413	0840	EN	65 39.6 N	025 15.5 W	GPS	85	12	5	CTD,LADCP,O2
3064	1	ROS	091413	1002	BE	65 45.0 N	025 38.1 W	GPS	270	5	12	CTD,LADCP,O2
3064	1	ROS	091413	1015	BO	65 44.9 N	025 38.4 W	GPS	270	5	12	CTD,LADCP,O2
3064	1	ROS	091413	1032	EN	65 44.9 N	025 38.4 W	GPS	270	5	12	CTD,LADCP,O2
3065	1	ROS	091413	1147	BE	65 49.9 N	025 59.7 W	GPS	222	3	11	CTD,LADCP,O2
3065	1	ROS	091413	1157	BO	65 49.9 N	025 59.8 W	GPS	222	3	11	CTD,LADCP,O2
3065	1	ROS	091413	1215	EN	65 50.0 N	026 00.0 W	GPS	222	3	11	CTD,LADCP,O2
3066	1	ROS	091413	1347	BE	65 56.0 N	026 28.8 W	GPS	286	4	12	CTD,LADCP,O2
3066	1	ROS	091413	1357	BO	65 56.0 N	026 28.9 W	GPS	286	4	12	CTD,LADCP,O2
3066	1	ROS	091413	1415	EN	65 56.0 N	026 29.2 W	GPS	286	4	12	CTD,LADCP,O2
3067	1	ROS	091413	1516	BE	66 01.0 N	026 47.6 W	GPS	450	5	16	CTD,LADCP,O2
3067	1	ROS	091413	1530	BO	66 01.0 N	026 48.0 W	GPS	450	5	16	CTD,LADCP,O2
3067	1	ROS	091413	1556	EN	66 01.1 N	026 48.5 W	GPS	450	5	16	CTD,LADCP,O2
3068	1	ROS	091413	1644	BE	66 05.1 N	027 03.1 W	GPS	650	6	17	CTD,LADCP,O2
3068	1	ROS	091413	1700	BO	66 05.3 N	027 03.7 W	GPS	650	6	17	CTD,LADCP,O2
3068	1	ROS	091413	1741	EN	66 06.0 N	027 05.9 W	GPS	650	6	17	CTD,LADCP,O2
3069	1	ROS	091413	1812	BE	66 08.8 N	027 14.6 W	GPS	502	4	17	CTD,LADCP,O2
3069	1	ROS	091413	1831	BO	66 09.2 N	027 15.4 W	GPS	502	4	17	CTD,LADCP,O2
3069	1	ROS	091413	1856	EN	66 09.2 N	027 16.3 W	GPS	502	4	17	CTD,LADCP,O2
3070	1	ROS	091413	2021	BE	66 14.7 N	027 44.8 W	GPS	471	3	14	CTD,LADCP,O2
3070	1	ROS	091413	2039	BO	66 14.9 N	027 46.2 W	GPS	471	3	14	CTD,LADCP,O2
3070	1	ROS	091413	2058	EN	66 15.0 N	027 47.0 W	GPS	471	3	14	CTD,LADCP,O2
3071	1	ROS	091413	2203	BE	66 19.7 N	028 07.8 W	GPS	340	5	13	CTD,LADCP,O2
3071	1	ROS	091413	2218	BO	66 19.9 N	028 08.5 W	GPS	340	5	13	CTD,LADCP,O2

3071	1	ROS	091413	2234	EN	66 20.0 N	028 09.0 W	GPS	340	5	13	CTD,LADCP,O2
3072	1	ROS	091413	2343	BE	66 24.8 N	028 31.0 W	GPS	299	5	10	CTD,LADCP,O2
3072	1	ROS	091413	2356	BO	66 25.1 N	028 31.6 W	GPS	299	5	10	CTD,LADCP,O2
3072	1	ROS	091513	0009	EN	66 25.2 N	028 32.0 W	GPS	299	5	10	CTD,LADCP,O2
3073	1	ROS	091513	0118	BE	66 29.7 N	028 53.9 W	GPS	320	6	10	CTD,LADCP,O2
3073	1	ROS	091513	0131	BO	66 29.9 N	028 54.6 W	GPS	320	6	10	CTD,LADCP,O2
3073	1	ROS	091513	0145	EN	66 30.0 N	028 55.0 W	GPS	320	6	10	CTD,LADCP,O2
3074	1	ROS	091513	0250	BE	66 34.8 N	029 15.8 W	GPS	308	5	10	CTD,LADCP,O2
3074	1	ROS	091513	0301	BO	66 35.0 N	029 16.3 W	GPS	308	5	10	CTD,LADCP,O2
3074	1	ROS	091513	0316	EN	66 35.1 N	029 16.8 W	GPS	308	5	10	CTD,LADCP,O2
3075	1	ROS	091513	0421	BE	66 39.7 N	029 38.3 W	GPS	297	3	10	CTD,LADCP,O2
3075	1	ROS	091513	0434	BO	66 39.9 N	029 38.8 W	GPS	297	3	10	CTD,LADCP,O2
3075	1	ROS	091513	0449	EN	66 39.9 N	029 38.9 W	GPS	297	3	10	CTD,LADCP,O2
3076	1	ROS	091513	0606	BE	66 44.9 N	030 02.2 W	GPS	326	5	12	CTD,LADCP,O2
3076	1	ROS	091513	0621	BO	66 45.1 N	030 02.9 W	GPS	326	5	12	CTD,LADCP,O2
3076	1	ROS	091513	0637	EN	66 45.1 N	030 03.1 W	GPS	326	5	12	CTD,LADCP,O2
3077	1	ROS	091513	0750	BE	66 49.9 N	030 26.3 W	GPS	411	7	14	CTD,LADCP,O2
3077	1	ROS	091513	0808	BO	66 49.9 N	030 26.9 W	GPS	411	7	14	CTD,LADCP,O2
3077	1	ROS	091513	0830	EN	66 50.0 N	030 27.0 W	GPS	411	7	14	CTD,LADCP,O2
3078	1	ROS	091513	0940	BE	66 55.0 N	030 49.5 W	GPS	581	6	17	CTD,LADCP,O2
3078	1	ROS	091513	0955	BO	66 55.0 N	030 49.7 W	GPS	581	6	17	CTD,LADCP,O2
3078	1	ROS	091513	1022	EN	66 55.0 N	030 50.1 W	GPS	581	6	17	CTD,LADCP,O2
3079	1	ROS	091513	1131	BE	66 59.9 N	031 12.5 W	GPS	360	11	14	CTD,LADCP,O2
3079	1	ROS	091513	1143	BO	66 59.9 N	031 12.7 W	GPS	360	11	14	CTD,LADCP,O2
3079	1	ROS	091513	1206	EN	66 59.9 N	031 13.3 W	GPS	360	11	14	CTD,LADCP,O2
3080	1	ROS	091513	1313	BE	67 04.8 N	031 35.8 W	GPS	297	9	12	CTD,LADCP,O2
3080	1	ROS	091513	1322	BO	67 04.8 N	031 35.9 W	GPS	297	9	12	CTD,LADCP,O2
3080	1	ROS	091513	1339	EN	67 04.7 N	031 36.3 W	GPS	297	9	12	CTD,LADCP,O2
3081	1	ROS	091513	1442	BE	67 09.7 N	031 58.4 W	GPS	300	5	13	CTD,LADCP,O2
3081	1	ROS	091513	1454	BO	67 09.9 N	031 59.1 W	GPS	300	5	13	CTD,LADCP,O2
3081	1	ROS	091513	1513	EN	67 09.9 N	031 59.5 W	GPS	300	5	13	CTD,LADCP,O2
3082	1	ROS	091513	1619	BE	67 15.0 N	032 21.7 W	GPS	366	3	14	CTD,LADCP,O2
3082	1	ROS	091513	1634	BO	67 15.0 N	032 22.6 W	GPS	366	3	14	CTD,LADCP,O2

3082	1	ROS	091513	1656	EN	67 14.9 N	032 23.0 W	GPS	366	3	14	CTD,LADCP,O2
3083	1	ROS	091513	1747	BE	67 19.3 N	032 41.5 W	GPS	434	6	13	CTD,LADCP,O2
3083	1	ROS	091513	1803	BO	67 19.5 N	032 42.4 W	GPS	434	6	13	CTD,LADCP,O2
3083	1	ROS	091513	1827	EN	67 19.5 N	032 42.6 W	GPS	434	6	13	CTD,LADCP,O2
3084	1	ROS	091513	1924	BE	67 23.8 N	033 02.5 W	GPS	321	6	9	CTD,LADCP,O2
3084	1	ROS	091513	1938	BO	67 24.1 N	033 02.4 W	GPS	321	6	9	CTD,LADCP,O2
3084	1	ROS	091513	1952	EN	67 24.1 N	033 02.3 W	GPS	321	6	9	CTD,LADCP,O2
3085	1	ROS	091513	2105	BE	67 19.5 N	032 42.4 W	GPS	440	6	10	CTD,LADCP,O2
3085	1	ROS	091513	2118	BO	67 19.4 N	032 42.3 W	GPS	440	6	10	CTD,LADCP,O2
3085	1	ROS	091513	2133	EN	67 19.4 N	032 42.4 W	GPS	440	6	10	CTD,LADCP,O2
3086	1	ROS	091513	2238	BE	67 15.3 N	032 23.0 W	GPS	360	5	8	CTD,LADCP,O2
3086	1	ROS	091513	2252	BO	67 15.1 N	032 22.7 W	GPS	360	5	8	CTD,LADCP,O2
3086	1	ROS	091513	2308	EN	67 14.8 N	032 23.1 W	GPS	360	5	8	CTD,LADCP,O2
3087	1	ROS	091613	0022	BE	67 09.9 N	031 59.5 W	GPS	303	6	7	CTD,LADCP,O2
3087	1	ROS	091613	0037	BO	67 09.8 N	031 59.0 W	GPS	303	6	7	CTD,LADCP,O2
3087	1	ROS	091613	0048	EN	67 09.8 N	031 59.2 W	GPS	303	6	7	CTD,LADCP,O2
3088	1	ROS	091613	0204	BE	67 04.8 N	031 36.5 W	GPS	292	5	7	CTD,LADCP,O2
3088	1	ROS	091613	0220	BO	67 04.8 N	031 36.0 W	GPS	292	5	7	CTD,LADCP,O2
3088	1	ROS	091613	0230	EN	67 04.7 N	031 36.2 W	GPS	292	5	7	CTD,LADCP,O2
3089	1	ROS	091613	0344	BE	67 00.0 N	031 13.3 W	GPS	358	3	9	CTD,LADCP,O2
3089	1	ROS	091613	0359	BO	66 59.9 N	031 12.9 W	GPS	358	3	9	CTD,LADCP,O2
3089	1	ROS	091613	0413	EN	66 59.8 N	031 13.1 W	GPS	358	3	9	CTD,LADCP,O2
3090	1	ROS	091613	0527	BE	66 55.1 N	030 50.4 W	GPS	581	1	13	CTD,LADCP,O2
3090	1	ROS	091613	0546	BO	66 55.1 N	030 49.6 W	GPS	581	1	13	CTD,LADCP,O2
3090	1	ROS	091613	0608	EN	66 55.0 N	030 49.7 W	GPS	581	1	13	CTD,LADCP,O2
3091	1	ROS	091613	0723	BE	66 50.0 N	030 27.3 W	GPS	411	6	13	CTD,LADCP,O2
3091	1	ROS	091613	0738	BO	66 50.0 N	030 26.7 W	GPS	411	6	13	CTD,LADCP,O2
3091	1	ROS	091613	0759	EN	66 50.0 N	030 26.5 W	GPS	411	6	13	CTD,LADCP,O2
3092	1	ROS	091613	0912	BE	66 45.1 N	030 03.0 W	GPS	328	4	14	CTD,LADCP,O2
3092	1	ROS	091613	0924	BO	66 45.0 N	030 02.6 W	GPS	328	4	14	CTD,LADCP,O2
3092	1	ROS	091613	0947	EN	66 44.9 N	030 02.4 W	GPS	328	4	14	CTD,LADCP,O2
3093	1	ROS	091613	1059	BE	66 39.9 N	029 38.9 W	GPS	297	5	9	CTD,LADCP,O2
3093	1	ROS	091613	1110	BO	66 39.8 N	029 38.6 W	GPS	297	5	9	CTD,LADCP,O2

3093	1	ROS	091613	1128	EN	66 39.9 N	029 38.6 W	GPS	297	5	9	CTD,LADCP,O2
3094	1	ROS	091613	1241	BE	66 35.0 N	029 16.5 W	GPS	304	4	12	CTD,LADCP,O2
3094	1	ROS	091613	1253	BO	66 34.9 N	029 16.1 W	GPS	304	4	12	CTD,LADCP,O2
3094	1	ROS	091613	1312	EN	66 34.9 N	029 16.4 W	GPS	304	4	12	CTD,LADCP,O2
3095	1	ROS	091613	1423	BE	66 30.0 N	028 54.4 W	GPS	324	7	12	CTD,LADCP,O2
3095	1	ROS	091613	1436	BO	66 29.9 N	028 54.2 W	GPS	324	7	12	CTD,LADCP,O2
3095	1	ROS	091613	1456	EN	66 29.7 N	028 54.9 W	GPS	324	7	12	CTD,LADCP,O2
3096	1	ROS	091613	1609	BE	66 25.1 N	028 32.0 W	GPS	300	5	11	CTD,LADCP,O2
3096	1	ROS	091613	1622	BO	66 25.1 N	028 31.7 W	GPS	300	5	11	CTD,LADCP,O2
3096	1	ROS	091613	1640	EN	66 25.1 N	028 32.1 W	GPS	300	5	11	CTD,LADCP,O2
3097	1	ROS	091613	1801	BE	66 20.0 N	028 08.5 W	GPS	341	5	12	CTD,LADCP,O2
3097	1	ROS	091613	1812	BO	66 20.0 N	028 08.1 W	GPS	341	5	12	CTD,LADCP,O2
3097	1	ROS	091613	1831	EN	66 20.0 N	028 08.1 W	GPS	341	5	12	CTD,LADCP,O2
3098	1	ROS	091613	1944	BE	66 14.9 N	027 46.0 W	GPS	473	6	13	CTD,LADCP,O2
3098	1	ROS	091613	2000	BO	66 14.9 N	027 45.4 W	GPS	473	6	13	CTD,LADCP,O2
3098	1	ROS	091613	2018	EN	66 14.9 N	027 45.7 W	GPS	473	6	13	CTD,LADCP,O2
3099	1	ROS	091613	2149	BE	66 09.1 N	027 15.7 W	GPS	517	5	14	CTD,LADCP,O2
3099	1	ROS	091613	2206	BO	66 09.0 N	027 15.4 W	GPS	517	5	14	CTD,LADCP,O2
3099	1	ROS	091613	2226	EN	66 08.6 N	027 16.2 W	GPS	517	5	14	CTD,LADCP,O2
3100	1	ROS	091613	2317	BE	66 05.1 N	027 03.5 W	GPS	655	5	16	CTD,LADCP,O2
3100	1	ROS	091613	2337	BO	66 04.8 N	027 03.4 W	GPS	655	5	16	CTD,LADCP,O2
3100	1	ROS	091713	0003	EN	66 04.3 N	027 04.5 W	GPS	655	5	16	CTD,LADCP,O2
3101	1	ROS	091713	0102	BE	66 01.0 N	026 48.7 W	GPS	444	4	11	CTD,LADCP,O2
3101	1	ROS	091713	0125	BO	66 00.8 N	026 48.1 W	GPS	444	4	11	CTD,LADCP,O2
3101	1	ROS	091713	0143	EN	66 00.8 N	026 47.7 W	GPS	444	4	11	CTD,LADCP,O2
3102	1	ROS	091713	0245	BE	65 56.0 N	026 29.4 W	GPS	284	4	9	CTD,LADCP,O2
3102	1	ROS	091713	0259	BO	65 55.8 N	026 29.0 W	GPS	284	4	9	CTD,LADCP,O2
3102	1	ROS	091713	0312	EN	65 55.8 N	026 29.1 W	GPS	284	4	9	CTD,LADCP,O2
3103	1	ROS	091713	0443	BE	65 49.9 N	026 00.6 W	GPS	223	4	8	CTD,LADCP,O2
3103	1	ROS	091713	0456	BO	65 49.8 N	026 00.1 W	GPS	223	4	8	CTD,LADCP,O2
3103	1	ROS	091713	0507	EN	65 49.8 N	026 00.5 W	GPS	223	4	8	CTD,LADCP,O2
3104	1	ROS	091713	0624	BE	65 45.0 N	025 39.3 W	GPS	275	3	9	CTD,LADCP,O2
3104	1	ROS	091713	0640	BO	65 44.9 N	025 38.6 W	GPS	275	3	9	CTD,LADCP,O2

3104	1	ROS	091713	0651	EN	65 44.9 N	025 38.8 W	GPS	275	3	9	CTD,LADCP,O2
3105	1	ROS	091713	0810	BE	65 39.9 N	025 16.3 W	GPS	84	6	7	CTD,LADCP,O2
3105	1	ROS	091713	0821	BO	65 39.9 N	025 15.9 W	GPS	84	6	7	CTD,LADCP,O2
3105	1	ROS	091713	0832	EN	65 40.0 N	025 15.8 W	GPS	84	6	7	CTD,LADCP,O2
3106	1	ROS	092013	0140	BE	64 24.4 N	014 03.5 W	GPS	106	4	4	CTD,LADCP,O2
3106	1	ROS	092013	0152	BO	64 24.4 N	014 02.9 W	GPS	106	4	4	CTD,LADCP,O2
3106	1	ROS	092013	0157	EN	64 24.4 N	014 02.9 W	GPS	106	4	4	CTD,LADCP,O2
3107	1	ROS	092013	0326	BE	64 17.1 N	013 36.3 W	GPS	164	5	5	CTD,LADCP,O2
3107	1	ROS	092013	0337	BO	64 16.8 N	013 36.3 W	GPS	164	5	5	CTD,LADCP,O2
3107	1	ROS	092013	0345	EN	64 16.7 N	013 36.6 W	GPS	164	5	5	CTD,LADCP,O2
3108	1	ROS	092013	0443	BE	64 14.1 N	013 21.6 W	GPS	175	5	5	CTD,LADCP,O2
3108	1	ROS	092013	0455	BO	64 13.9 N	013 21.2 W	GPS	175	5	5	CTD,LADCP,O2
3108	1	ROS	092013	0503	EN	64 13.8 N	013 21.5 W	GPS	175	5	5	CTD,LADCP,O2
3109	1	ROS	092013	0618	BE	64 08.1 N	013 03.3 W	GPS	164	5	8	CTD,LADCP,O2
3109	1	ROS	092013	0632	BO	64 08.0 N	013 03.1 W	GPS	164	5	8	CTD,LADCP,O2
3109	1	ROS	092013	0644	EN	64 08.1 N	013 03.3 W	GPS	164	5	8	CTD,LADCP,O2
3110	1	ROS	092013	0731	BE	64 05.0 N	012 52.2 W	GPS	573	7	16	CTD,LADCP,O2
3110	1	ROS	092013	0747	BO	64 05.1 N	012 51.7 W	GPS	573	7	16	CTD,LADCP,O2
3110	1	ROS	092013	0816	EN	64 05.7 N	012 51.2 W	GPS	573	7	16	CTD,LADCP,O2
3111	1	ROS	092013	0915	BE	64 01.0 N	012 38.1 W	GPS	563	5	16	CTD,LADCP,O2
3111	1	ROS	092013	0931	BO	64 01.1 N	012 37.6 W	GPS	563	5	16	CTD,LADCP,O2
3111	1	ROS	092013	0957	EN	64 01.3 N	012 36.9 W	GPS	563	5	16	CTD,LADCP,O2
3112	1	ROS	092013	1056	BE	63 57.0 N	012 19.9 W	GPS	460	6	14	CTD,LADCP,O2
3112	1	ROS	092013	1111	BO	63 57.1 N	012 20.1 W	GPS	460	6	14	CTD,LADCP,O2
3112	1	ROS	092013	1133	EN	63 57.2 N	012 20.1 W	GPS	460	6	14	CTD,LADCP,O2
3113	1	ROS	092013	1247	BE	63 50.0 N	011 59.9 W	GPS	386	5	12	CTD,LADCP,O2
3113	1	ROS	092013	1259	BO	63 50.0 N	011 59.9 W	GPS	386	5	12	CTD,LADCP,O2
3113	1	ROS	092013	1319	EN	63 49.8 N	012 00.3 W	GPS	386	5	12	CTD,LADCP,O2
3114	1	ROS	092013	1426	BE	63 44.0 N	011 39.9 W	GPS	346	4	13	CTD,LADCP,O2
3114	1	ROS	092013	1437	BO	63 43.8 N	011 39.9 W	GPS	346	4	13	CTD,LADCP,O2
3114	1	ROS	092013	1458	EN	63 43.6 N	011 40.2 W	GPS	346	4	13	CTD,LADCP,O2
3115	1	ROS	092013	1627	BE	63 36.1 N	011 15.0 W	GPS	305	5	11	CTD,LADCP,O2
3115	1	ROS	092013	1639	BO	63 36.0 N	011 15.1 W	GPS	305	5	11	CTD,LADCP,O2

3115	1	ROS	092013	1658	EN	63 36.0 N	011 15.3 W	GPS	305	5	11	CTD,LADCP,O2
3116	1	ROS	092013	1831	BE	63 29.1 N	010 49.3 W	GPS	442	4	15	CTD,LADCP,O2
3116	1	ROS	092013	1847	BO	63 29.0 N	010 49.0 W	GPS	442	4	15	CTD,LADCP,O2
3116	1	ROS	092013	1912	EN	63 29.3 N	010 49.0 W	GPS	442	4	15	CTD,LADCP,O2
3117	1	ROS	092013	2048	BE	63 20.2 N	010 25.1 W	GPS	328	2	14	CTD,LADCP,O2
3117	1	ROS	092013	2104	BO	63 20.0 N	010 24.6 W	GPS	328	2	14	CTD,LADCP,O2
3117	1	ROS	092013	2124	EN	63 20.2 N	010 23.7 W	GPS	328	2	14	CTD,LADCP,O2
3118	1	ROS	092013	2246	BE	63 14.2 N	009 58.4 W	GPS	486	5	18	CTD,LADCP,O2
3118	1	ROS	092013	2304	BO	63 13.9 N	009 57.3 W	GPS	486	5	18	CTD,LADCP,O2
3118	1	ROS	092013	2330	EN	63 13.8 N	009 56.9 W	GPS	486	5	18	CTD,LADCP,O2
3119	1	ROS	092113	0045	BE	63 06.2 N	009 38.2 W	GPS	491	4	17	CTD,LADCP,O2
3119	1	ROS	092113	0101	BO	63 05.9 N	009 37.5 W	GPS	491	4	17	CTD,LADCP,O2
3119	1	ROS	092113	0126	EN	63 05.8 N	009 37.1 W	GPS	491	4	17	CTD,LADCP,O2
3120	1	ROS	092113	0259	BE	62 58.1 N	009 09.3 W	GPS	442	6	16	CTD,LADCP,O2
3120	1	ROS	092113	0316	BO	62 57.7 N	009 08.8 W	GPS	442	6	16	CTD,LADCP,O2
3120	1	ROS	092113	0338	EN	62 57.3 N	009 09.3 W	GPS	442	6	16	CTD,LADCP,O2
3121	1	ROS	092113	0455	BE	62 51.2 N	008 50.3 W	GPS	463	4	17	CTD,LADCP,O2
3121	1	ROS	092113	0515	BO	62 50.9 N	008 50.1 W	GPS	463	4	17	CTD,LADCP,O2
3121	1	ROS	092113	0539	EN	62 50.6 N	008 50.6 W	GPS	463	4	17	CTD,LADCP,O2
3122	1	ROS	092113	0709	BE	62 44.1 N	008 26.9 W	GPS	482	5	15	CTD,LADCP,O2
3122	1	ROS	092113	0724	BO	62 44.0 N	008 26.7 W	GPS	482	5	15	CTD,LADCP,O2
3122	1	ROS	092113	0748	EN	62 44.1 N	008 26.3 W	GPS	482	5	15	CTD,LADCP,O2
3123	1	ROS	092113	0926	BE	62 35.0 N	008 02.0 W	GPS	416	4	13	CTD,LADCP,O2
3123	1	ROS	092113	0941	BO	62 35.2 N	008 01.8 W	GPS	416	4	13	CTD,LADCP,O2
3123	1	ROS	092113	1004	EN	62 35.5 N	008 00.9 W	GPS	416	4	13	CTD,LADCP,O2
3124	1	ROS	092113	1137	BE	62 26.1 N	007 38.9 W	GPS	103	6	6	CTD,LADCP,O2
3124	1	ROS	092113	1147	BO	62 26.0 N	007 38.8 W	GPS	103	6	6	CTD,LADCP,O2
3124	1	ROS	092113	1159	EN	62 25.9 N	007 37.9 W	GPS	103	6	6	CTD,LADCP,O2
3125	1	ROS	092113	1311	BE	62 20.0 N	007 15.4 W	GPS	90	6	6	CTD,LADCP,O2
3125	1	ROS	092113	1324	BO	62 20.0 N	007 14.8 W	GPS	90	6	6	CTD,LADCP,O2
3125	1	ROS	092113	1335	EN	62 20.2 N	007 14.8 W	GPS	90	6	6	CTD,LADCP,O2
3126	1	ROS	092113	2042	BE	61 50.2 N	006 21.7 W	GPS	77	5	5	CTD,LADCP,O2
3126	1	ROS	092113	2052	BO	61 50.0 N	006 21.9 W	GPS	77	5	5	CTD,LADCP,O2

3126	1	ROS	092113	2059	EN	61 50.1 N	006 21.8 W	GPS	77	5	5	CTD,LADCP,O2
3127	1	ROS	092113	2225	BE	61 42.7 N	005 58.0 W	GPS	302	4	13	CTD,LADCP,O2
3127	1	ROS	092113	2239	BO	61 42.6 N	005 57.3 W	GPS	302	4	13	CTD,LADCP,O2
3127	1	ROS	092113	2258	EN	61 42.7 N	005 56.9 W	GPS	302	4	13	CTD,LADCP,O2
3128	1	ROS	092213	0010	BE	61 37.1 N	005 36.4 W	GPS	316	3	12	CTD,LADCP,O2
3128	1	ROS	092213	0026	BO	61 37.0 N	005 35.4 W	GPS	316	3	12	CTD,LADCP,O2
3128	1	ROS	092213	0044	EN	61 37.2 N	005 35.4 W	GPS	316	3	12	CTD,LADCP,O2
3129	1	ROS	092213	0150	BE	61 31.2 N	005 19.4 W	GPS	286	6	12	CTD,LADCP,O2
3129	1	ROS	092213	0204	BO	61 30.9 N	005 18.8 W	GPS	286	6	12	CTD,LADCP,O2
3129	1	ROS	092213	0220	EN	61 30.8 N	005 18.6 W	GPS	286	6	12	CTD,LADCP,O2
3130	1	ROS	092213	0325	BE	61 25.1 N	005 01.4 W	GPS	224	5	11	CTD,LADCP,O2
3130	1	ROS	092213	0338	BO	61 24.8 N	005 00.9 W	GPS	224	5	11	CTD,LADCP,O2
3130	1	ROS	092213	0354	EN	61 24.7 N	005 01.0 W	GPS	224	5	11	CTD,LADCP,O2
3131	1	ROS	092213	0503	BE	61 20.1 N	004 43.5 W	GPS	732	9	19	CTD,LADCP,O2
3131	1	ROS	092213	0530	BO	61 19.9 N	004 43.2 W	GPS	732	9	19	CTD,LADCP,O2
3131	1	ROS	092213	0603	EN	61 19.7 N	004 43.2 W	GPS	732	9	19	CTD,LADCP,O2
3132	1	ROS	092213	0755	BE	61 16.0 N	004 27.9 W	GPS	1054	5	19	CTD,LADCP,O2
3132	1	ROS	092213	0821	BO	61 16.3 N	004 27.5 W	GPS	1054	5	19	CTD,LADCP,O2
3132	1	ROS	092213	0859	EN	61 16.6 N	004 26.4 W	GPS	1054	5	19	CTD,LADCP,O2
3133	1	ROS	092213	0953	BE	61 12.0 N	004 17.9 W	GPS	1080	4	19	CTD,LADCP,O2
3133	1	ROS	092213	1019	BO	61 12.2 N	004 17.4 W	GPS	1080	4	19	CTD,LADCP,O2
3133	1	ROS	092213	1059	EN	61 12.9 N	004 16.4 W	GPS	1080	4	19	CTD,LADCP,O2
3134	1	ROS	092213	1152	BE	61 08.0 N	004 04.0 W	GPS	1121	5	21	CTD,LADCP,O2
3134	1	ROS	092213	1217	BO	61 08.1 N	004 03.6 W	GPS	1121	5	21	CTD,LADCP,O2
3134	1	ROS	092213	1256	EN	61 08.3 N	004 03.2 W	GPS	1121	5	21	CTD,LADCP,O2
3135	1	ROS	092213	1342	BE	61 04.1 N	003 52.1 W	GPS	1147	4	20	CTD,LADCP,O2
3135	1	ROS	092213	1409	BO	61 03.9 N	003 52.1 W	GPS	1147	4	20	CTD,LADCP,O2
3135	1	ROS	092213	1446	EN	61 03.6 N	003 52.5 W	GPS	1147	4	20	CTD,LADCP,O2
3136	1	ROS	092213	1542	BE	60 59.1 N	003 38.1 W	GPS	1101	5	19	CTD,LADCP,O2
3136	1	ROS	092213	1616	BO	60 58.9 N	003 38.9 W	GPS	1101	5	19	CTD,LADCP,O2
3136	1	ROS	092213	1654	EN	60 58.7 N	003 39.5 W	GPS	1101	5	19	CTD,LADCP,O2
3137	1	ROS	092213	1813	BE	60 52.1 N	003 18.5 W	GPS	683	4	19	CTD,LADCP,O2
3137	1	ROS	092213	1835	BO	60 52.0 N	003 17.9 W	GPS	683	4	19	CTD,LADCP,O2

3137	1	ROS	092213	1906	EN	60 52.3 N	003 17.8 W	GPS	683	4	19	CTD,LADCP,O2
3138	1	ROS	092213	2034	BE	60 45.0 N	002 55.5 W	GPS	354	4	11	CTD,LADCP,O2
3138	1	ROS	092213	2051	BO	60 45.0 N	002 54.9 W	GPS	354	4	11	CTD,LADCP,O2
3138	1	ROS	092213	2107	EN	60 45.1 N	002 54.8 W	GPS	354	4	11	CTD,LADCP,O2
3139	1	ROS	092213	2228	BE	60 38.1 N	002 36.5 W	GPS	133	5	7	CTD,LADCP,O2
3139	1	ROS	092213	2240	BO	60 38.0 N	002 35.9 W	GPS	133	5	7	CTD,LADCP,O2
3139	1	ROS	092213	2249	EN	60 38.1 N	002 35.8 W	GPS	133	5	7	CTD,LADCP,O2
3140	1	ROS	092313	0028	BE	60 31.0 N	002 16.4 W	GPS	141	5	7	CTD,LADCP,O2
3140	1	ROS	092313	0039	BO	60 30.9 N	002 15.9 W	GPS	141	5	7	CTD,LADCP,O2
3140	1	ROS	092313	0049	EN	60 30.9 N	002 16.0 W	GPS	141	5	7	CTD,LADCP,O2
3141	1	ROS	092313	0208	BE	60 25.0 N	001 55.5 W	GPS	112	5	6	CTD,LADCP,O2
3141	1	ROS	092313	0218	BO	60 24.9 N	001 55.0 W	GPS	112	5	6	CTD,LADCP,O2
3141	1	ROS	092313	0225	EN	60 24.9 N	001 55.0 W	GPS	112	5	6	CTD,LADCP,O2

Table 2

	O2, ml/l
Total amount of analyzed samples	1273
Number of duplicates	77
Mean difference of duplicates	0.01
Min difference of duplicates	0.00
Max difference of duplicates	0.03
Median difference of duplicates	0.005
Standard deviation of difference	0.005
Accuracy	0.07%

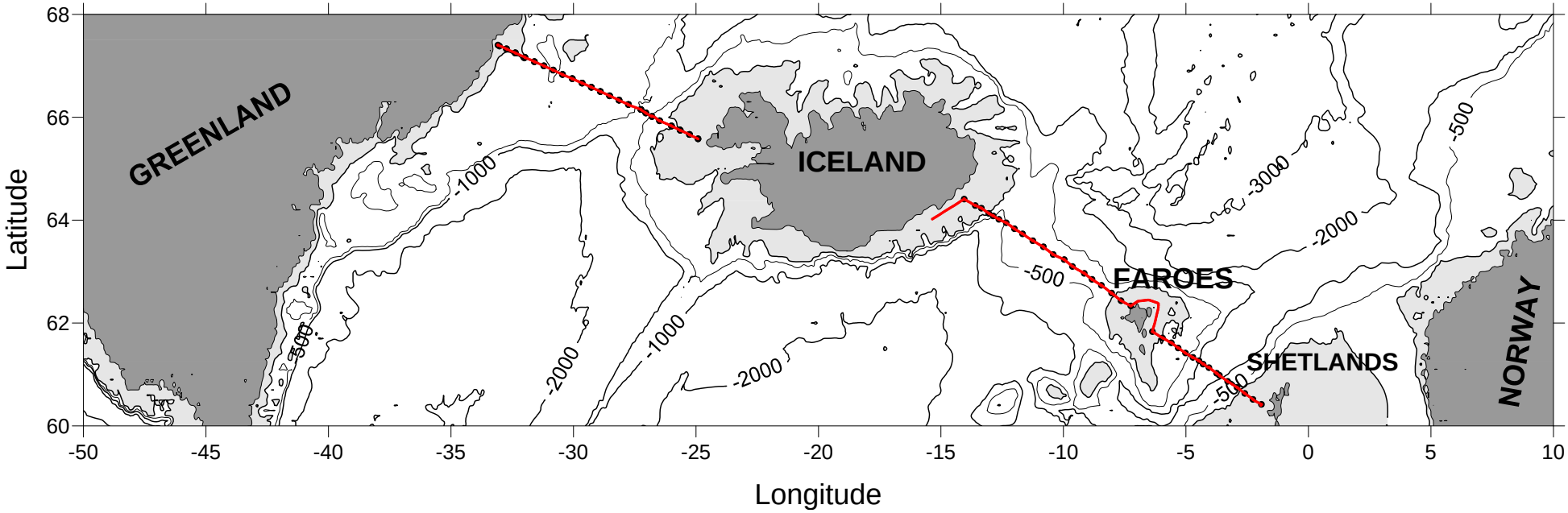

Fig. 1 Station locations (black circles) and ship track (in red). The shelf area with depth less than 200 m is shaded.

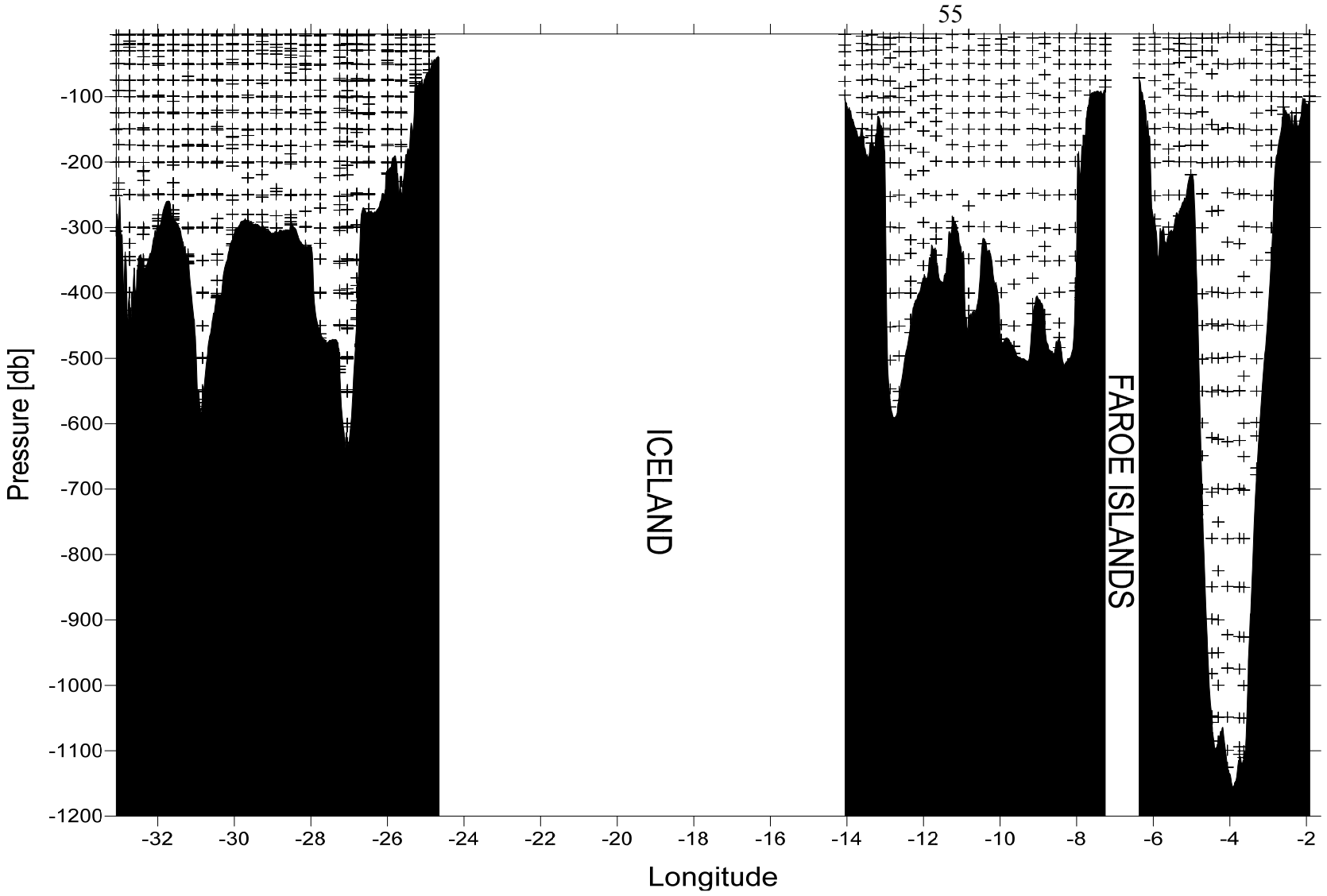

Figure 2. Vertical distribution of samples along the sill sections.

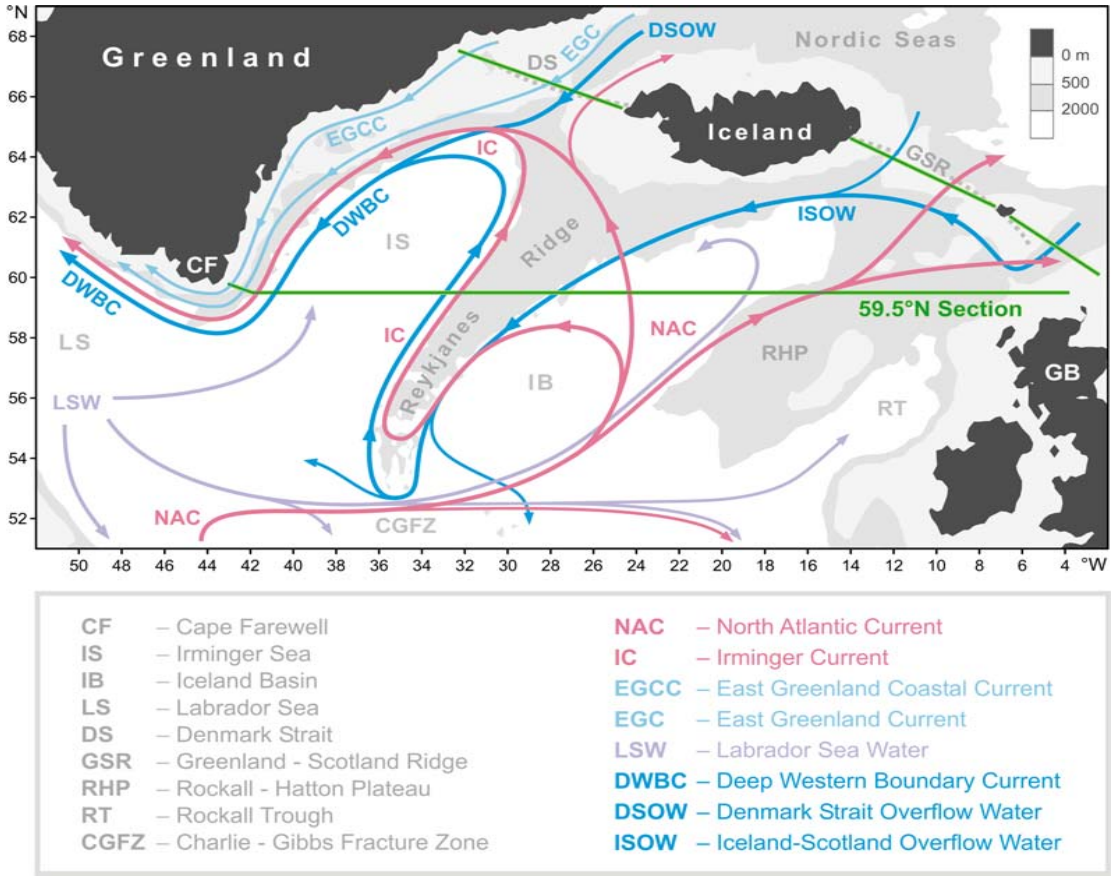

Figure 3. Schematic diagram of the large-scale circulation in the northern North Atlantic compiled from [Schmitz and McCartney, 1993; Schott and Brandt, 2007; Sutherland and Pickart, 2008; Lherminier et al., 2010]. Abbreviations for the main topographic features, currents and water masses are explained in the legend. The nominal locations of the 59.5°N hydrographic section (1997 – present) and sections across the straits between Greenland, Iceland, Faeroe and Shetland Islands (2011 – present) are shown with the solid green lines.

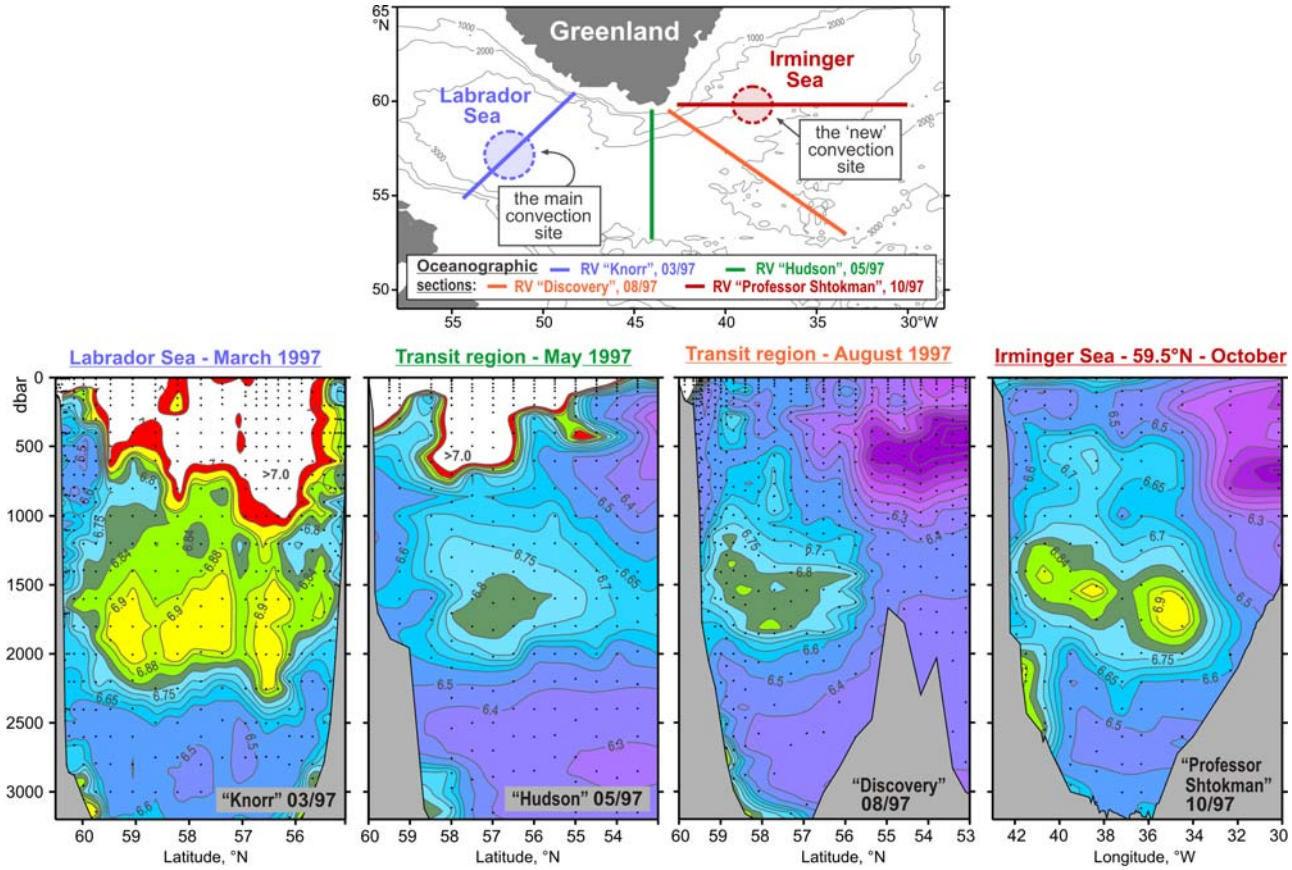

Figure 4. Oxygen concentrations (ml/l) in the water column (lower panel) as observed in March–October 1997 in four hydrographic sections (upper panel) ending nearby the southern tip of Greenland. A separate oxygen maximum in the LSW layer (1000–2000 m) in the Irminger Sea at 59.5°N strongly implies local convective renewal of LSW before 1997. Adapted from [Falina et al., 2007].

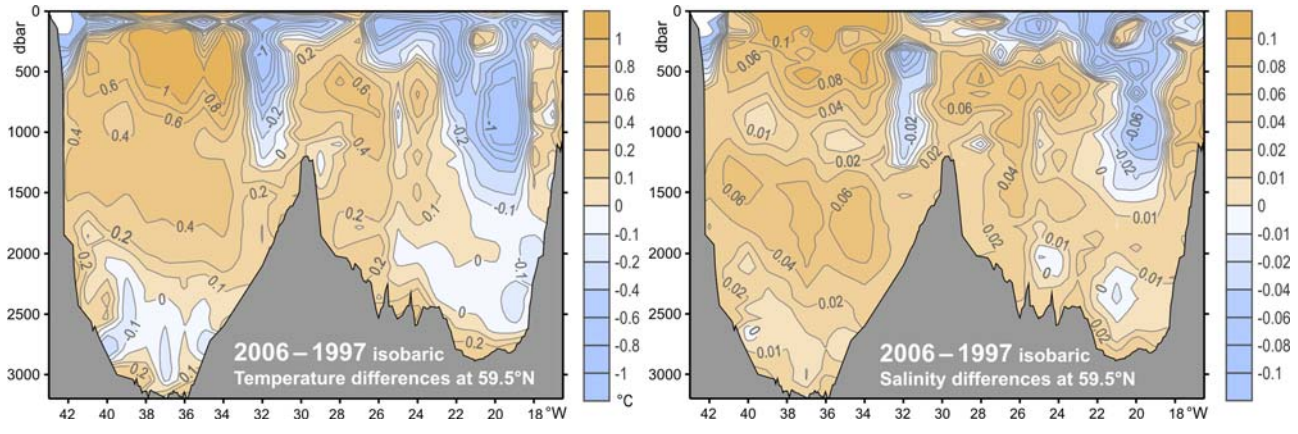

Figure 5. Warming and salinification in the northern North Atlantic between the mid-1990s and mid-2000s, as observed at 59.5°N. The figure shows the 2006–1997 temperature (°C, left) and salinity (right) differences on isobaric surfaces in the Irminger Sea and Iceland Basin. Adapted from [Sarafanov et al., 2007].

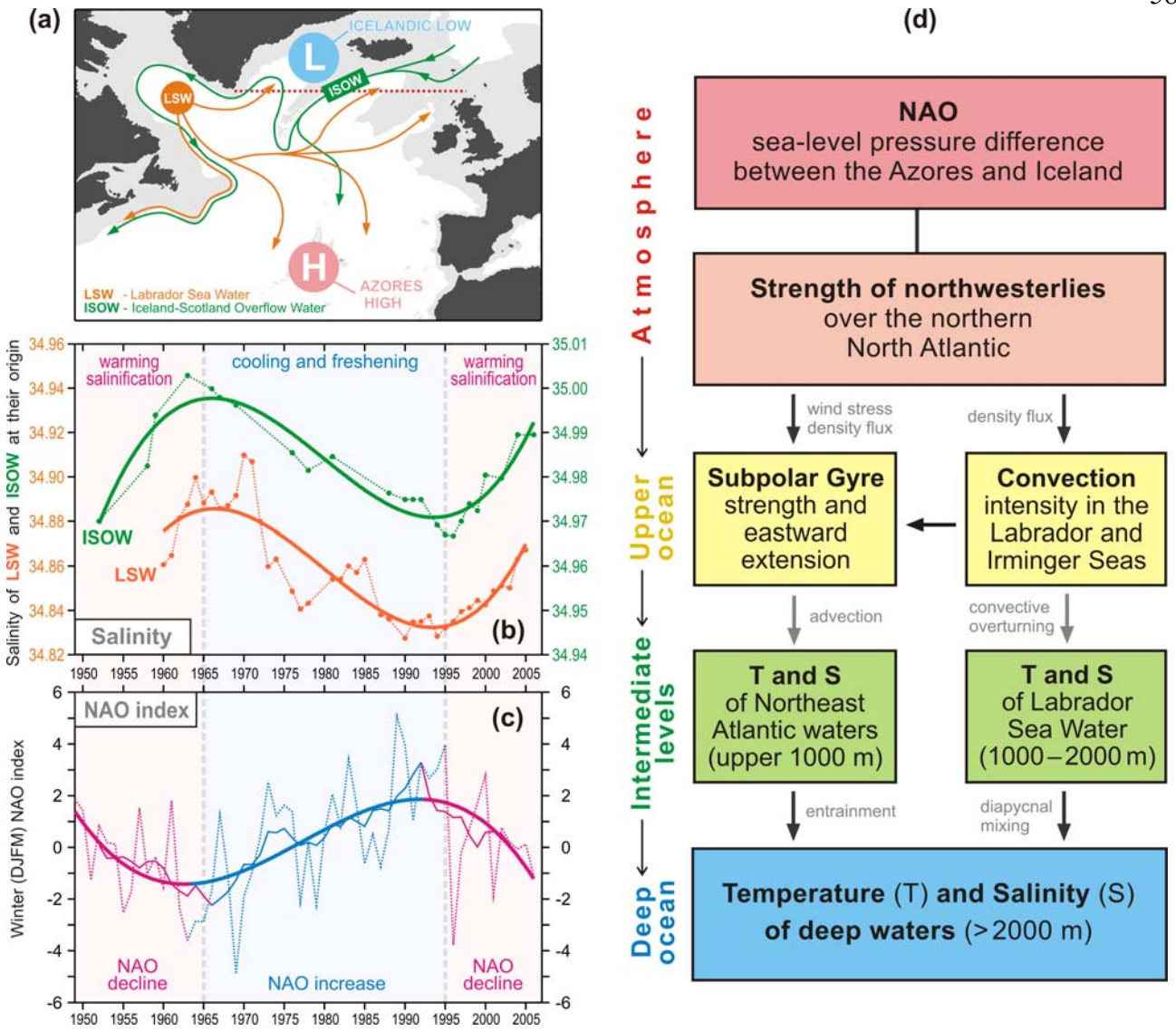

Figure 6. Coherence of the decadal salinity changes (1950s – 2000s) of the intermediate (LSW) and deep (ISOW) waters in the northern North Atlantic and their link to the North Atlantic Oscillation (NAO) index. **(a)** Schematic representation of the LSW and ISOW pathways and locations of the Icelandic Low (L) and Azores High (H) centers constituting the NAO dipole pattern. The red dotted line indicates the 59.5°N transatlantic section. **(b)** Salinity time series for LSW in the Labrador Sea [Yashayaev, 2007] and ISOW in the Iceland basin [Boessenkool et al., 2007; Sarafanov et al., 2007] overlaid by the third order polynomial fits. **(c)** Time series of the winter NAO index, after [Hurrell, 1995], overlaid by 7-year running mean and third order polynomial fit. **(d)** Mechanism of the NAO effect on the decadal changes in temperature (T) and salinity (S) of the northern North Atlantic intermediate and deep waters. Positive / negative links shown with the dark / light grey arrows mean that changes in 'causative' and 'consequential' characteristics have the same / opposite sign(s). The overall effect of the NAO on T and S of the in the water column is negative: persistent NAO decline leads to warming and salinification of the water masses and vice versa, as shown in (b) and (c). Adapted from [Sarafanov, 2009].

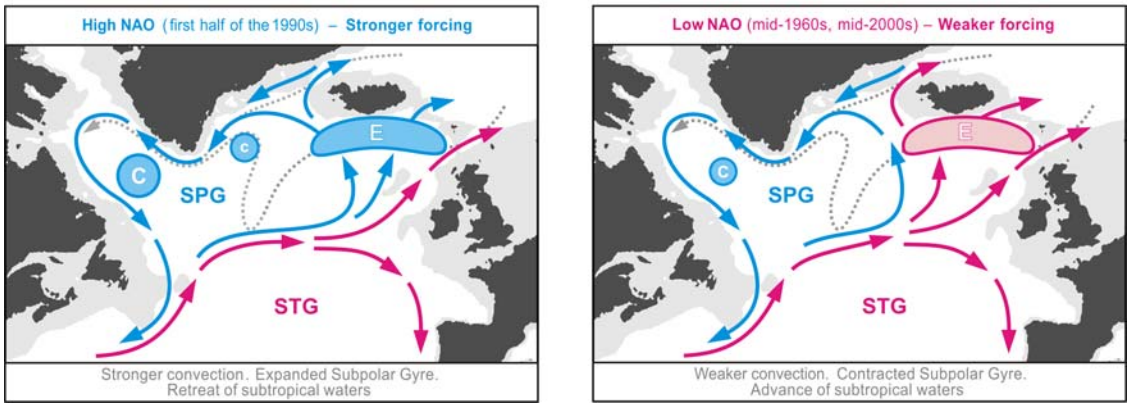

Figure 7. Schematic representation of the upper-ocean circulation and convection intensity in the northern North Atlantic under high (left) and low (right) NAO conditions. Blue (magenta) solid arrows indicate the upper-ocean flows with higher fraction of colder fresher subpolar (warmer saltier subtropical) waters. The main pathways of the Nordic overflow-derived deep waters are shown with the dotted curves. "C" and "E" symbols are used to denote, respectively, the deep convection sites and the domain, where the Atlantic waters are entrained into ISOW. Larger (smaller) circles indicate stronger (weaker) convection. SPG and STG – the subpolar and subtropical gyres, respectively. Adapted from [Sarafanov, 2009].

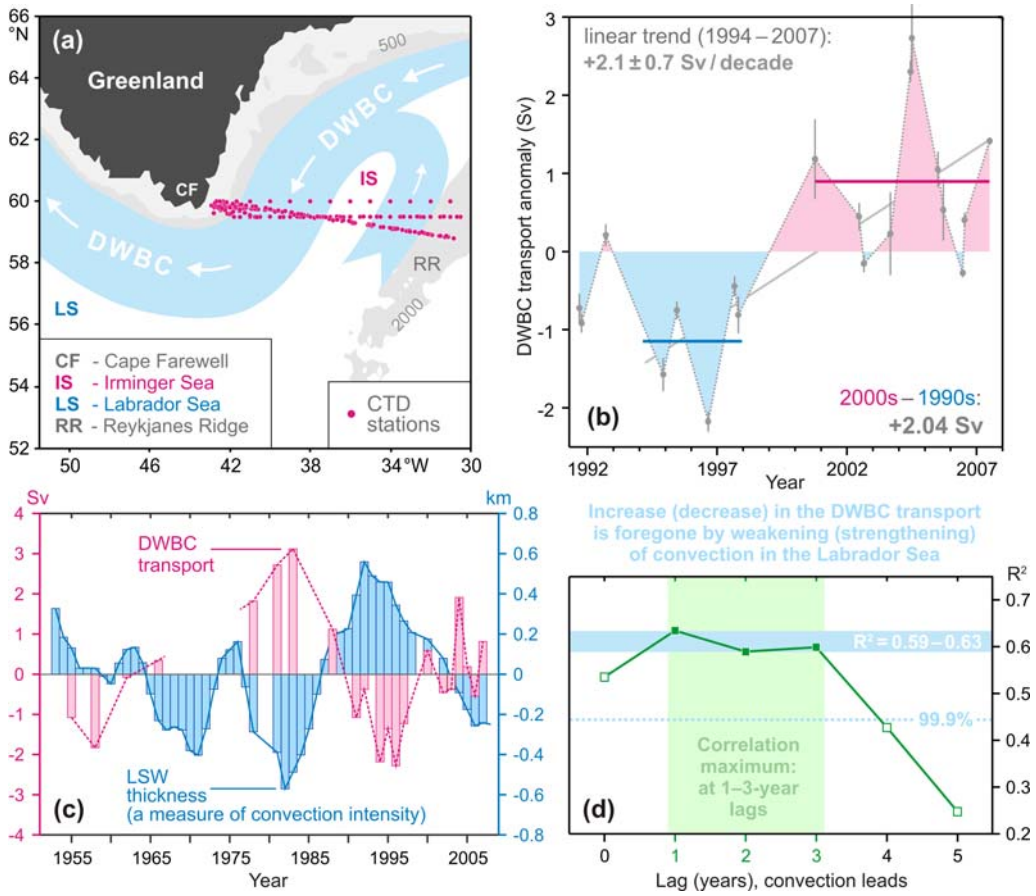

Figure 8. The Deep Western Boundary Current (DWBC) transport variability and its link to the convection intensity in the Labrador Sea. **(a)** Locations of the hydrographic sections (1991–2007) and schematic of the deep water circulation in the Irminger Sea. **(b)** The DWBC transport anomalies at Cape Farewell in 1991–2007, 1 Sv = 10^6 m^3 s^{-1}. The 1994–1997 and 2000–2007 mean anomalies and the 1994–2007 linear trend are shown. **(c)** Anomalies of the DWBC transport at Cape Farewell and the Labrador Sea Water (LSW) thickness in the Labrador Sea in the 1950s–2000s. **(d)** Correlation coefficient (R^2) for the two times series shown in **(c)** at the 0–5-year lag, the LSW thickness leads. The correlation maximum is achieved at the 1–3-year lag. The DWBC transport anomalies in the southern Irminger Sea are foregone by the convection intensity anomalies in the Labrador Sea. Adapted from [Sarafanov et al., 2009].

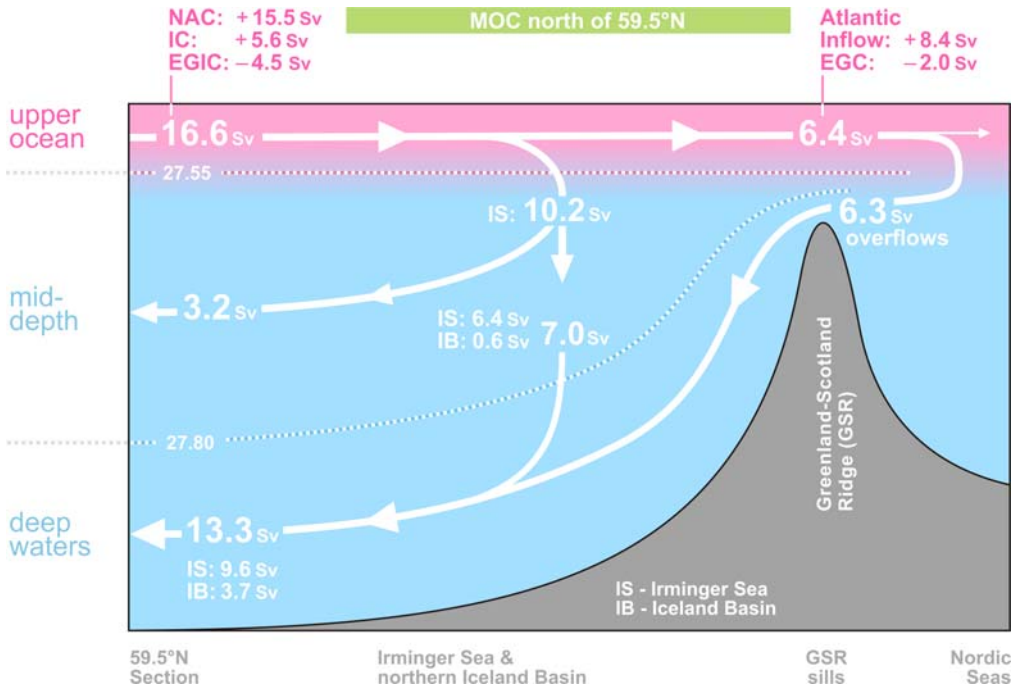

Figure 9. Schematic diagram of the Meridional Overturning Circulation (MOC) at the northern periphery of the Atlantic Ocean, northeast of Cape Farewell. The dotted lines refer to the σ_0 isopycnals 27.55 and 27.80. The arrows denote the integral meridional and diapycnal volume fluxes. Where the signs are specified, the positive (negative) transports are northward (southward). The NAC and EGIC transports in the upper layer ($\sigma_0 < 27.55$) at 59.5°N are the throughputs accounting for the recirculations. EGIC – the East Greenland / Irminger Current – refers to the upper part of the Western Boundary Current. Other abbreviations are explained in the legend to **Figure 3**. Adapted from [Sarafanov et al., 2012].

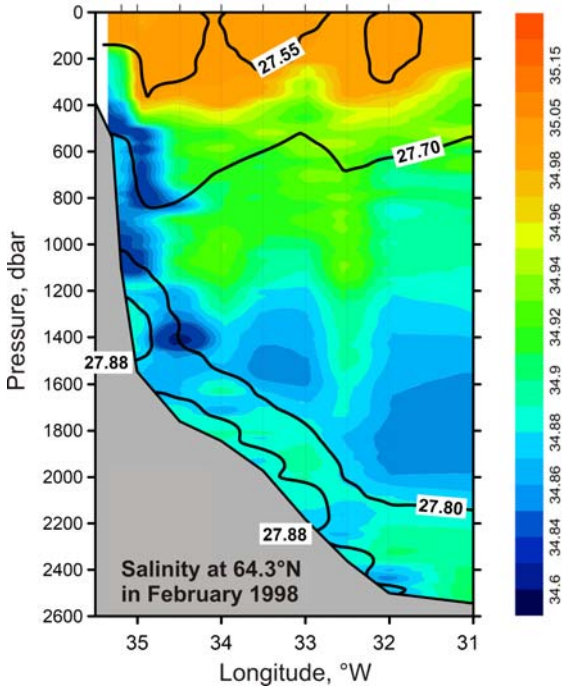

Figure 10. Salinity observed in the northwestern Irminger Sea at 64.3°N in February 1998. The σ_0 isopycnals 27.55, 27.70, 27.80 and 27.88 are plotted as the thick black lines; the station locations are marked with the ticks on the top axis. The plot shows fresh dense waters descending (cascading) down the continental slope of Greenland down to the LSW layer ($27.70 < \sigma_0 < 27.80$) and the layer of the Nordic Seas overflow-derived deep waters ($\sigma_0 > 27.80$). Adapted from [Falina et al., 2012].

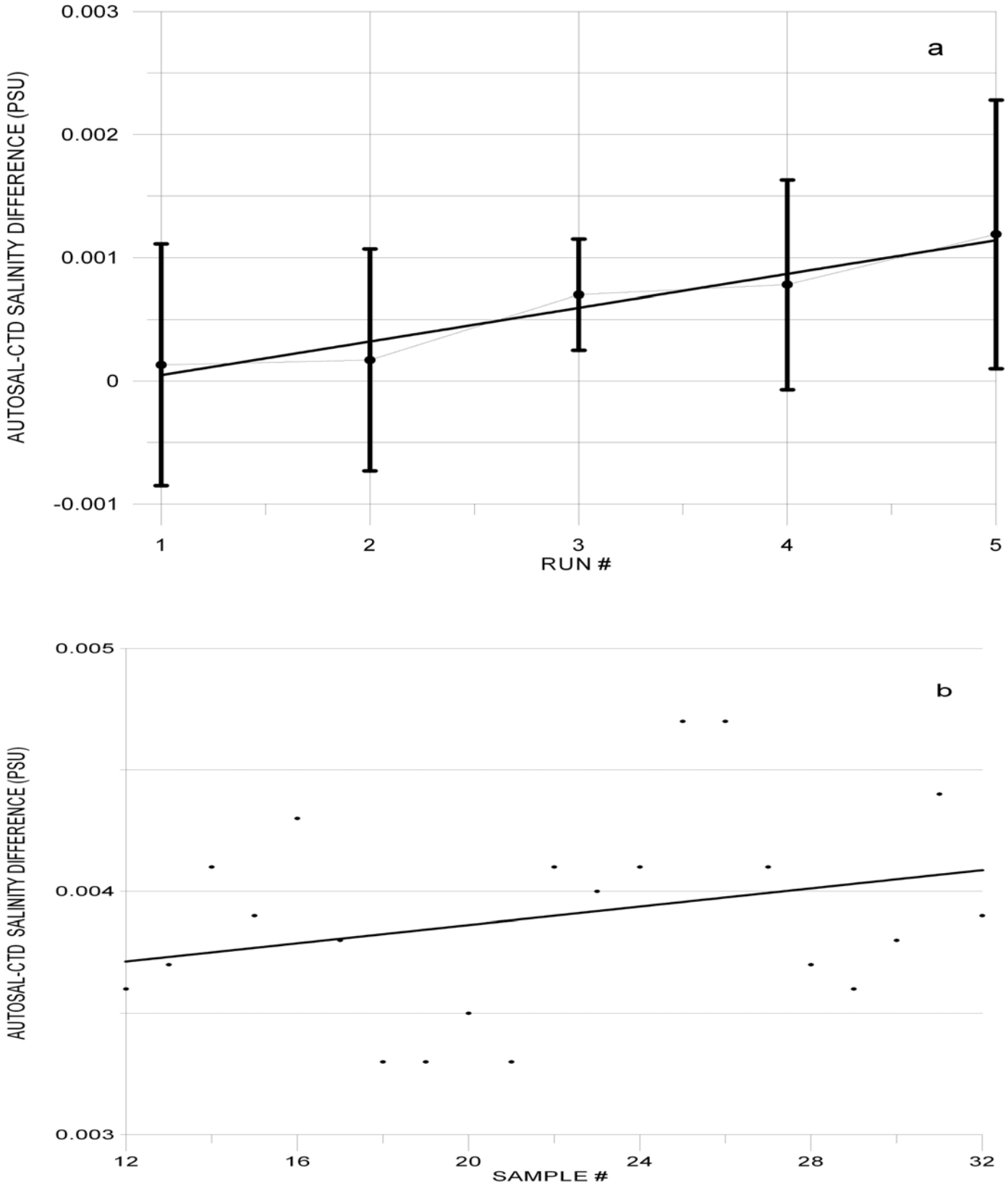

Figure 11 Autosal 8400B CTD salinity offset for the primary conductivity sensors (a) SBE 9P 0743 based on 246 salinity samples (5 runs) (b) SBE 9P 0767 based on 20 salinity samples during 42 cruise of R/V *Akademik Ioffe*. Vertical bars show standard deviation of each run. Thick black line denotes linear fit.

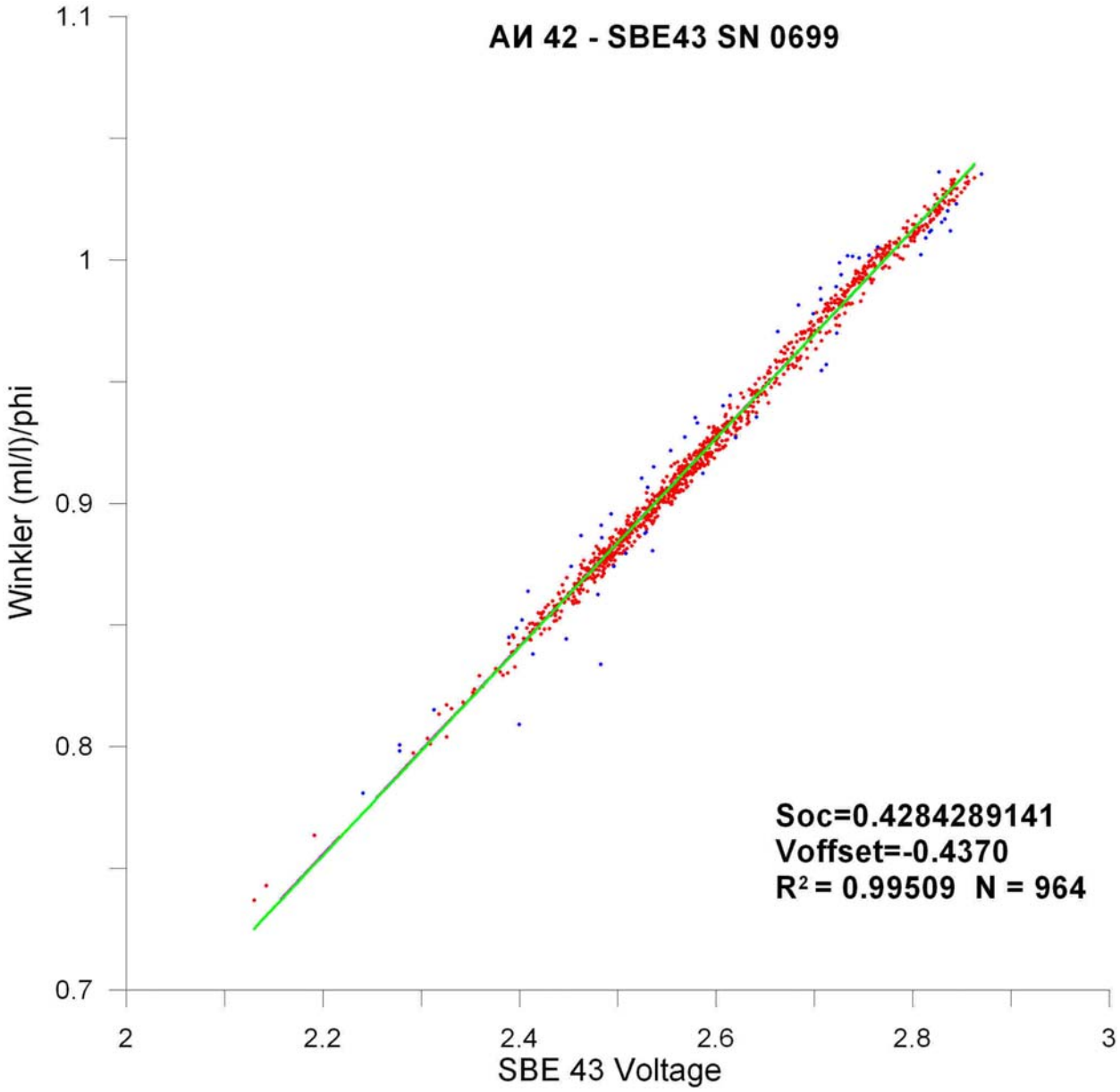

Figure 12 Regression line for Winkler oxygen divided by φ versus SBE 43 output voltage the sill sections.

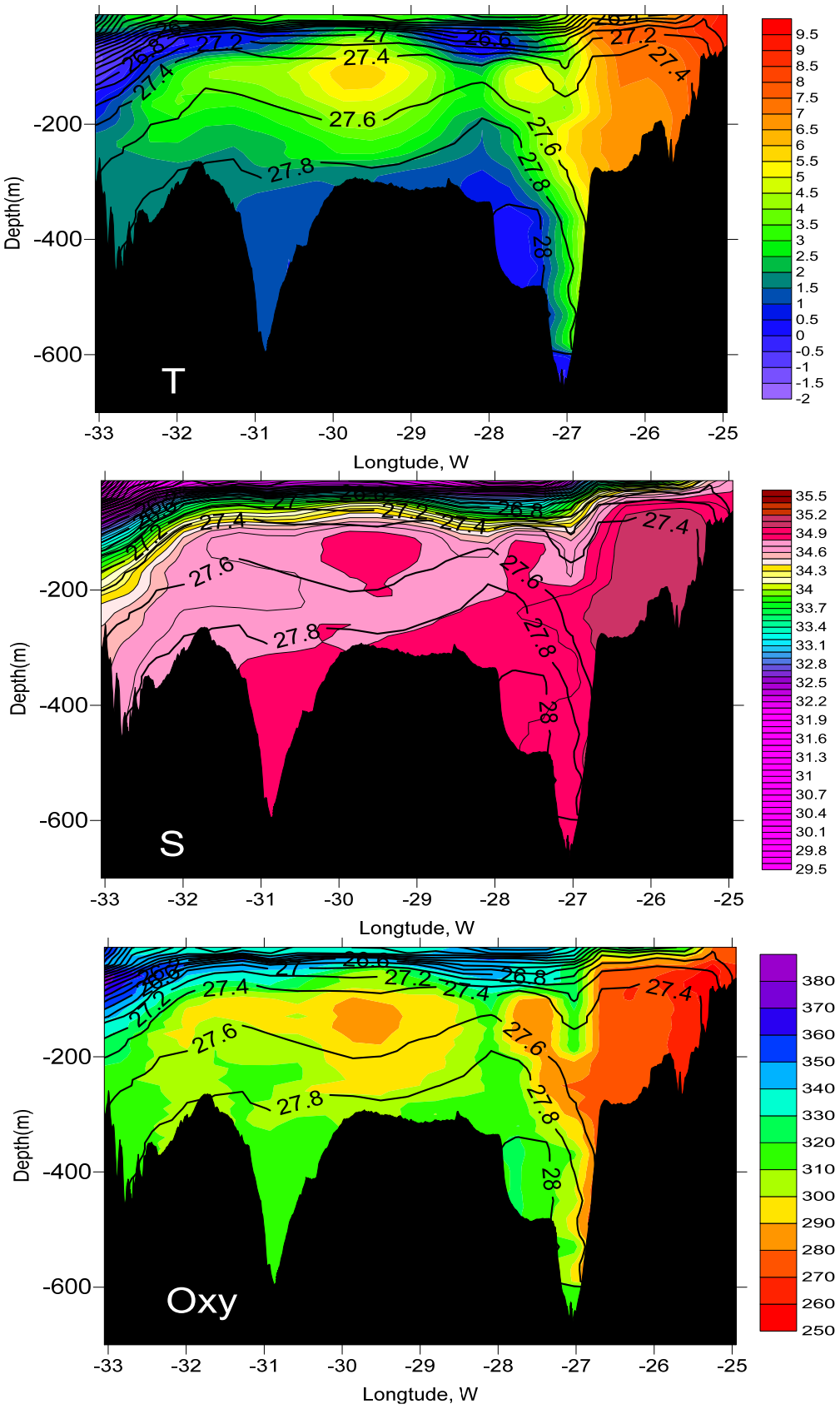

Figure 13 The vertical distribution of (a) potential temperature and (b) salinity and (c) dissolved oxygen between Greenland and Iceland 12-14 September 2013. Density is shown in black.

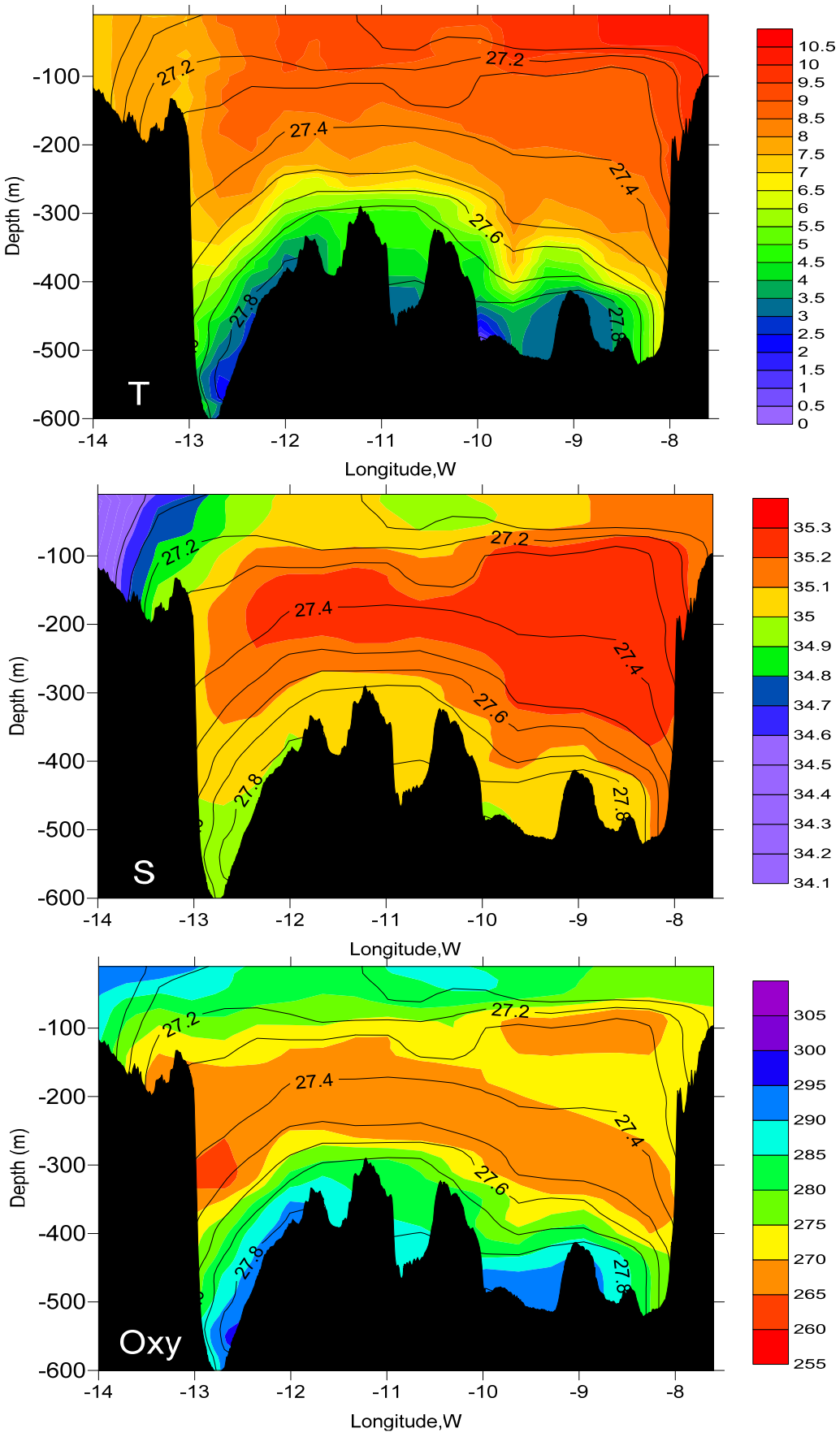

Figure 14 The vertical distribution of (a) potential temperature and (b) salinity and (c) dissolved oxygen between Iceland and Faroe Islands 20-21 September 2013. Density is shown in black.

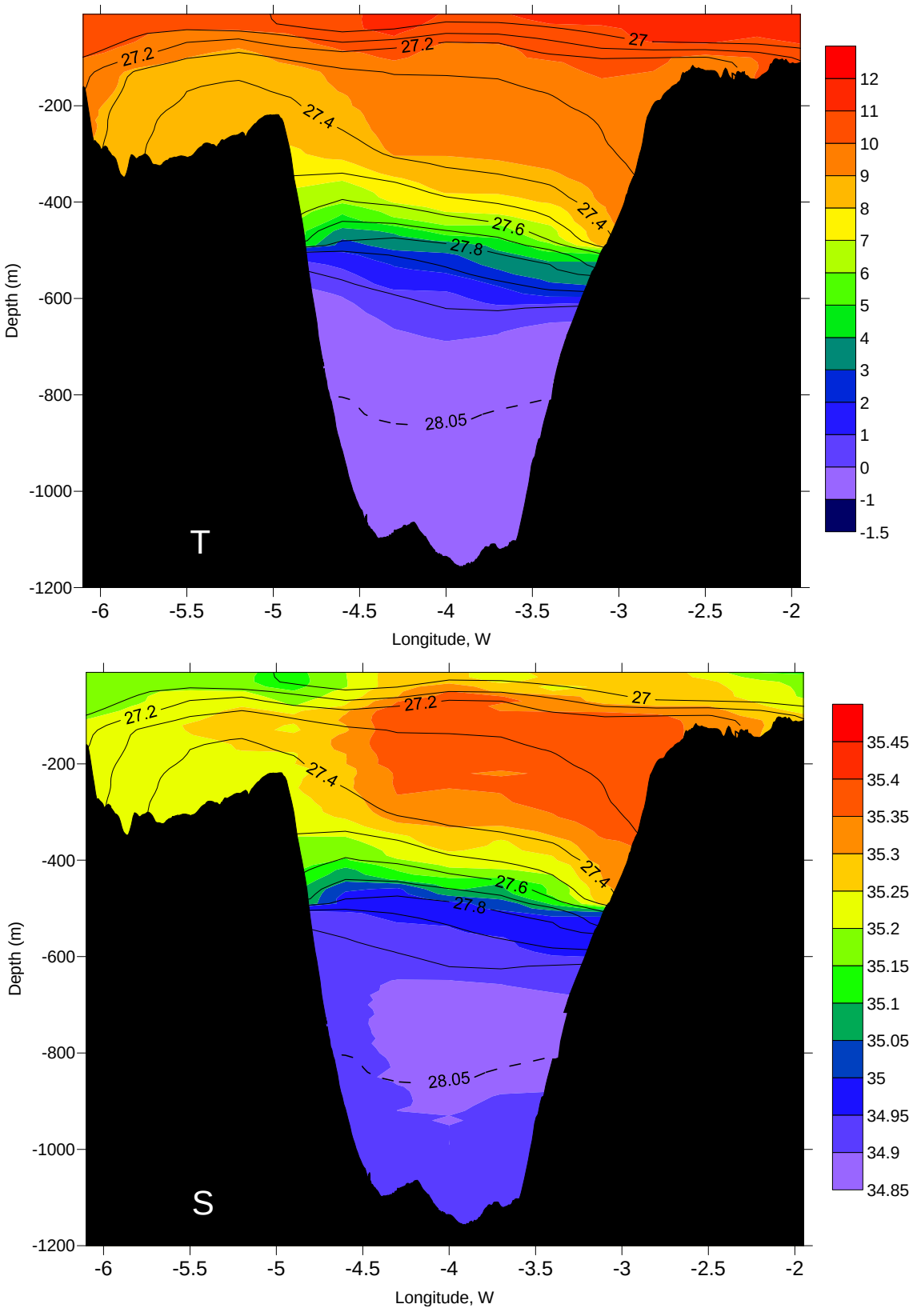

Figure 15 The vertical distribution of (a) potential temperature and (b) salinity between Shetlands and Faroe Islands 21-23 September 2013. Density is shown in black.